83
SUR/FIN

American Electroplaters' Society SUR/FIN '83

70th Annual Technical Conference

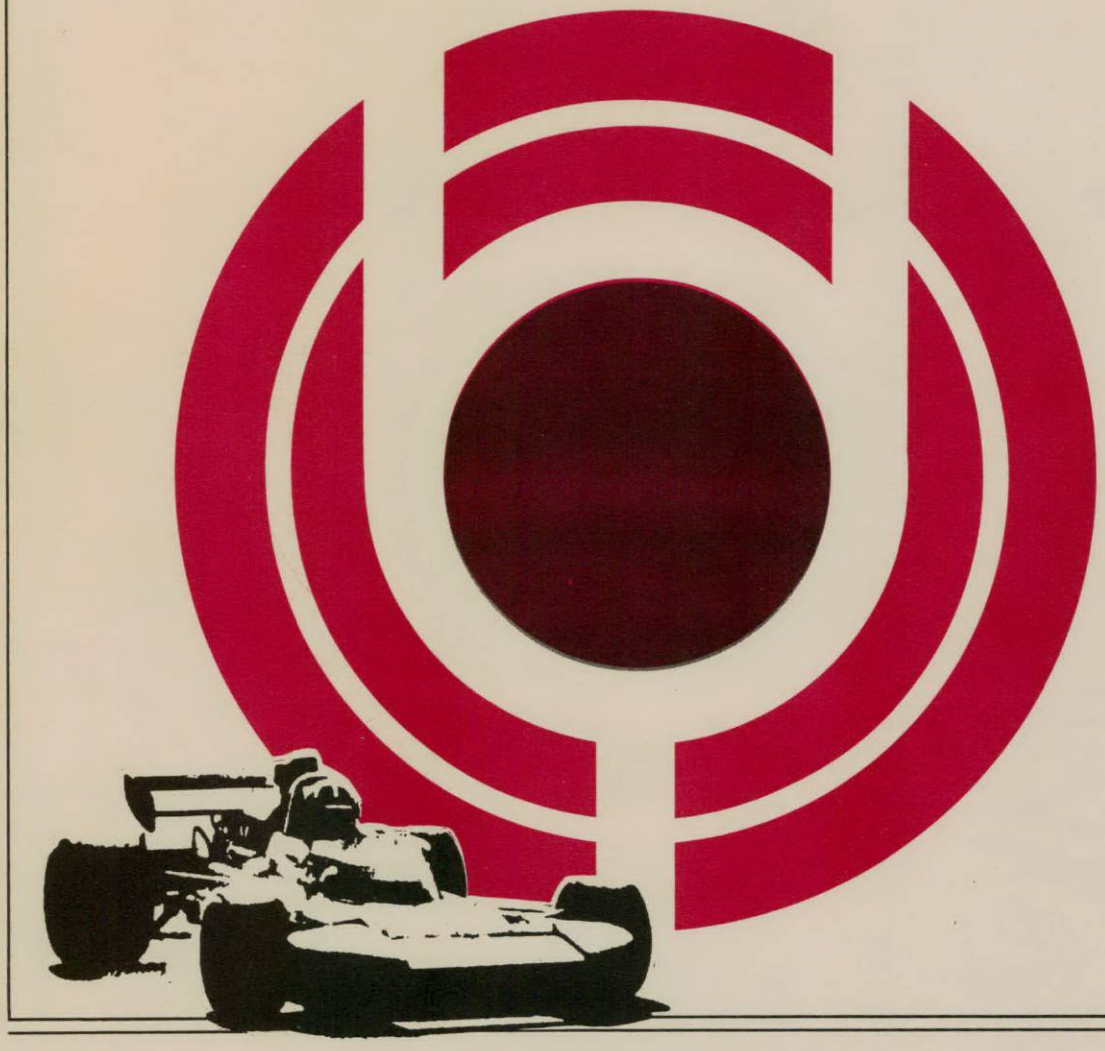

June 27-30, 1983
Hyatt Regency Indianapolis and
The Indiana Convention - Exposition Center
Indianapolis, IN

SESSION A - Research

AMERICAN ELECTROPLATERS' SOCIETY, INC.

70TH ANNUAL TECHNICAL CONFERENCE - INDIANAPOLIS, IN

RESEARCH

SESSION A

Page No.

A-1

Research Session A

Interdiffusion of Electrodeposits with Copper Substrates

Suryanarayana Kaja, Dr. Howard W. Pickering and Dr. William Bitler
The Pennsylvania State University
University Park, PA

INTERDIFFUSION OF ELECTRODEPOSITS WITH COPPER SUBSTRATES

S. Kaja, H. W. Pickering and W. R. Bitler
Metallurgy Program
Department of Materials Science and Engineering
The Pennsylvania State University
University Park, PA 16802 U.S.A.

This is a report on a portion of the research sponsored by AES under AES Reserach Project 50. Project 50 is concerned with those deposits of direct interest to the electronics industry i.e. principally gold and possible substitutes for gold.

Prior work under this project has concentrated on the effectiveness of various barrier materials in reducing the interdiffusion of gold with its substrate. At the conclusion of this paper some of the more recent results in this area will be reported. The major discussion, however, will center on our recent findings with regard to the interdiffusion of palladium with copper substrates. For your easy reference the palladium results will be continually compared with similar results for the nickel-copper system. Since nickel is frequently used as a barrier in the copper-gold system this will give some basis for comparing a copper palladium system with a copper-nickel barrier-gold system.

A blistering problem was encountered with the palladium electrodeposits most probably arising from hydrogen codeposited with the palladium. In view of this problem, conventional diffusion couples of wrought copper and wrought palladium were prepared and diffusion annealed at various temperatures ranging from 450°C to 900°C. The concentration profiles of these samples were determined from microprobe scans, Boltzmann-Matano analyzed and D_{chem} determined as a function of composition. An Arrhenius plot of the results showed linear behavior at low and high temperatures with the break occurring at about 750°C. See Figure 1. The composition dependence is consistent with what one would expect on the basis of the phase diagram i.e., the diffusivity decreases near the Pd rich end when the solidus temperature starts to rise appreciably.

Some qualitative observations with regard to the interdiffusion of the palladium electrodeposited on copper follow. Deposits of 1/2, 1 and 2 μm thick were diffusion annealed at temperatures ranging from 350°C to 750°C. At temperatures below 750°C the blistering of the thicker deposits, the 1 and 2 μm thick ones, was so severe that no diffusion results were obtainable Above 750°C the blistering problem disappeared. Below 750°C the thinnest samples, the 1/2 μm thick samples, were sufficiently adherent that diffusion behavior could be noted. These samples show very rapid interdiffusion. Three days at 350°C was sufficient to allow enough copper penetration of the palladium electrodeposit such that the naked eye could detect the color change in the palladium deposit. (No such color change could be detected on nickel deposits simultaneously diffusion annealed in the same capsule). Subsequent examination of the palladium electrodeposits by the transmission electro microscope (TEM) showed that the grain size of the palladium deposits was very small ∿100-500 A. Such small grain size and grain boundary diffusion

would explain the rapid penetration of copper through the palladium deposits. The effective diffusivity for these samples is much larger than the comparable data appearing in Figure 1 for wrought Pd-Cu couples.

Finally results on hexavalent chromium and semi-bright cobalt indicate that either of these would be a more effective diffusion barrier than nickel when used between copper and gold.

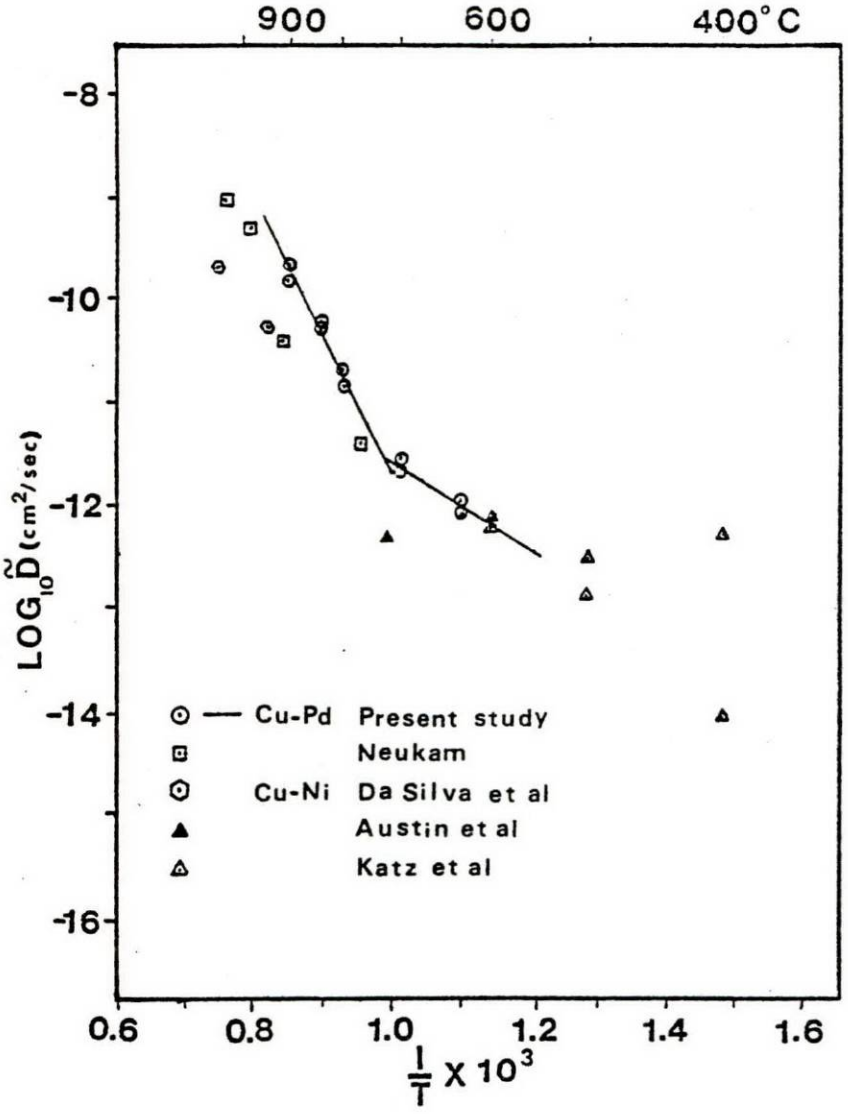

Figure 1.

Logarithm of Interdiffusivity vs. reciprocal temperature for Cu/Pd and Cu/Ni systems calculated at 50 atom percent copper, except Katz et al at 60 wt%.

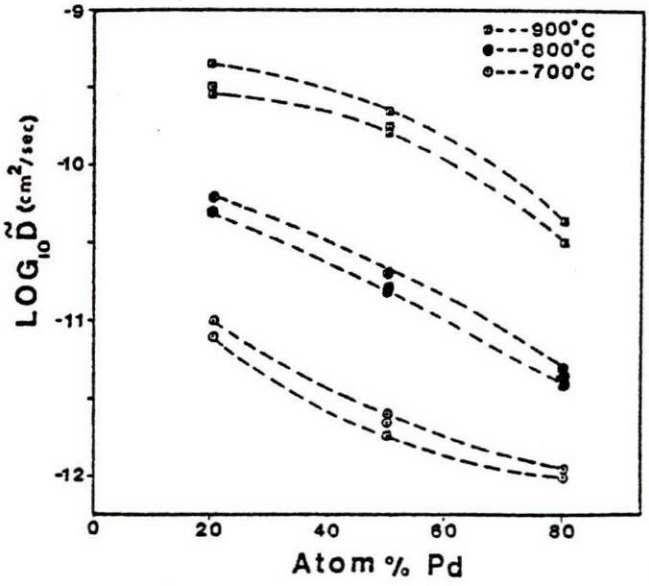

Figure 2.

Logarithm of Interdiffusivity vs. atom percent Pd for Cu/Pd system.

A-2

Research Session A

Deposition of Nickel Chromium Alloys

Dr. David S. Lashmore
National Bureau of Standards
Washington, DC

DEPOSITION OF NICKEL CHROMIUM ALLOYS

D. S. Lashmore
Center for Materials Science
National Bureau of Standards
Washington, D.C. 20234

ABSTRACT

Nickel chromium alloys have been deposited from electrolytes containing the chloride salts of nickel and chromium. Coatings greater than 75 microns thick have been deposited with the chromium content controllable from about 0.1 Wt% to 60 Wt.% by appropriate choice of the deposition parameters. The surface morphology, corrosion performance and structure have been correlated with the deposition conditions. Applications of pulsed current deposition techniques have yielded improvements in surface morphology which is explained in terms of the changes in diffusion length occurring under pulsed conditions. Crystal phases were found in the coating deposited by direct current deposition which were different from those formed under pulsed current conditions. Preliminary potentiodynamic anodic polorization measurements of corrosion in both chloride and in 1 normal sulfuric acid indicate that these electrodeposited coatings may be significantly more corrosion resistant than comparable wrought alloys of similar chromium content. This unusual corrosion performance may be due to the presence of layers of strong chromium composition gradients.

INTRODUCTION

Electrodeposited coatings of nickel chromium alloys have a number of properties which would be likely to attract wide commercial interest if an appropriate deposition process existed. It has been reported by Kruger and McBee (1) for materials with chromium contents greater than about 20 Wt. % that the surface would be covered with an amorphous passive film that would be unusually resistant to corrosion. This finding has been observed for a number of stainless steels and has been discussed in depth by Revesz and Kruger (2). The wear performance especially at higher temperatures might also be expected to be comparable to other commonly used coatings such as hard chromium (3) and because the coating can be applied using electrodeposition techniques, the adhesion between the coating and the substrate can be comparable to the cohesive strength of the substrate, with the additional advantage that the coatings can be applied to the interior surfaces of very small parts. Protective wear and corrosion resistant coatings are becoming increasingly important to alleviate the dependence of the United States on strategic materials particularly important among these are chromium and cobalt. The United States imports almost 100% of its chromium and 97% of its cobalt from countries that can not be relied upon (4). Since chromium is used mainly for its corrosion properties, a surface phenomena, coatings containing chromium offer an important means of dealing with the critical materials problem. By using corrosion *resistent coatings the entire part no longer has to contain large quantities of the strategic material.

There have been numerous attempts to electrodeposit alloys of nickel with chromium and nickel with molybdenum. Many of these attempts were reviewed by Chisom (5) who concluded that there is presently no commercial process capable of depositing the alloy. Typical of the problems encountered by the earlier investigators were (a) the inability to build up a coating of thickness greater than 25 microns, (b) inability to incorporate significant amounts of chromium into the deposit and (c) poor morphology, that is coatings which are highly stressed or dendritic. More recent studies of Stromatt (6) and Hayashi (7,8) seem to have been more successful. Hayashi's study was of an iron nickel chromium process which made use of electrolytes containing trivalent forms of chromium and various complexing agents. Pulsed electrodeposition of the ternary iron nickel chromium alloys were reported by Hayashi (8) who found that direct current coatings exhibited structures much different from those observed for pulsed deposited coatings.

PROCESSES DEVELOPMENT

A process was formulated using trivalent chromium which was chosen because it is far less oxidizing in solution than the hexavalent form of the ion and so is more tolerant of organic complexing agents. This is rather important as, based on the results of previous investigators organic, complexing agents would seem to be required for the successful deposition of the alloy. It should also be noted that the trivalent ion requires less energy to reduce to the metal than the hexavalent. Trivalent

ions are also far easier to treat when present in electroplating wastes that are hexavalent ions. Hexavalent electrolytes have been reported to be successful for the deposition of nickel chromium alloys by Shluger and Kazakov (9) and more recently for cobalt chromium alloys by Gilshinski and Yahalom (10). Experience in our laboratory has shown us that thick coatings of a nickel chromium alloy are very difficult to obtain from hexavalent electrolytes under normal conditions.

In deposition from trivalent chromium electrolytes, formation of the hexavalent chromium ion at the anode should be avoided both to avoid oxidizing the complexing agents as well as to maximize the current efficiency. To help accomplish this in the process described here ammonium bromide was added to the solution as the bromide oxidizes at a lower potential than does the trivalent chromium. Probably an iodine salt also could be used. This of course results in the liberation of some bromine at the anode. Further to aid in the reduction of any hexavalent chromium which may be formed, formic acid was added to the solution. Formic acid is a known catalyst (11) for the reduction of chromium from hexavalent solutions. It should not be overlooked that the formic acid may play a role in the reduction of the trivalent ion. A number of complexing agents for both nickel and chromium were investigated, the most successful was found to be glycolic acid. Glycine was also found to be successful but its instability under long term use made it unacceptable. Boric acid was found to be essential and may act to minimize hydrolysis reactions or to act as a buffer through some mechanism which is not clear.

mount of chromium in the electrolyte was optimized by first fixing the concentration of nickel hexahydrate at 30 g/L and varying the chromium chloride hexahydrate from 0 to 130 g/L. Measurements of chromium content of the coating were made by X-ray fluorescence using the procedure described by Rasberry and Heinrich (12). It was found that the chromium content of the deposit exhibited a peak at a solution content of 100 g/L of chromium hexahydride as is shown in Fig. 1a. The solubility of glycolic acid is very large and much more has been added to the solution than is necessary to complex the chromium and the nickel. No effect on chromium content of the deposit was observed by varying the amount of glycolic acid in the solution.

The amount of chromium in the electrolyte was then fixed at 100 g/L and the nickel content varied. The chromium content in the coating was found to peak at 30 g/L nickel, as shown in Fig. 1b which was then fixed for future experiments. The maximum chromium current efficiency for the deposition of chromium was found to be around 14.4 percent. This value compares with the the current efficiency of typical hexavalent chromium plating solutions which is usually around 13%.

The dependence of the current efficiency for chromium deposition on the current density is shown in Fig. 2. At about 20 A/dm^2 direct current deposition yields coatings of about 18 Wt. % chromium.

The amount of chromium in the alloy was measured as a function of temperature and pH of the electrolyte and the results are shown in Fig. 3. As the temperature increases, the amount of

mium in the alloy gradually decreases. This result may indicate that the diffusion of chromium ions to the cathode is less than nickel and most probably the activation energy for diffusion of chromium is less than that for nickel.

In order to determine the effect of pH on the amount of chromium in the alloy, a number of coatings were made at various pH values and their chromium contents were measured using the X-ray fluorescence technique discussed above. The results are shown in Fig. 4 where the current efficiency for chromium deposition is plotted as a function of pH and a function of temperature. The efficiency goes through a minimum at around 55 ^{o}C and at a pH of 2. At a temperature of 30 ^{o}C deposits containing over 18 Wt.% chromium were produced by direct current deposition. Significant improvements in deposit morphology were obtained by pulsed electrodeposition and are discussed below.

The overall current efficiency was measured as a function of temperature for three values of pH. These results are shown in Fig. 5 . The cross-over of the curve for pH1 indicates that the deposition of hydrogen is favored at higher temperatures. The appearance of the coating at pH 2 is also better.

Based on these studies along with Hull cell measurements, which will not be discussed here, an electrolyte formulation was developed and is given below:

::

NiCl2 6H2O	30	g/L
CrCl3 6H2O	100	
Formic acid	35	ml/L
Glycolic acid	50	g/L
NH4Br	80	g/L
Boric Acid	40	
Temperature	30	oC
pH	2.0	

::

PULSED CURRENT DEPOSITION

Pulsed current deposition using the waveform shown in Fig. 6 was undertaken in order to determine the effect on coating morphology and composition. Duty cycle in the following discussion is defined as time on divided by the sum of time on and time off as:

$$(1) \quad \text{Duty Cycle} = \frac{\text{Time On}}{\text{Time On + Time Off}}$$

Current density is the value during the On Time. The effects of pulsing the current in the above manner were discussed by Ibl(13,14) and Che(15,16) and a number of investigators have found important effects on both morphology and composition (17,18). During the On time, the concentration of both nickel and chromium ions is reduced within a certain diffusion distance. This diffusion layer pulsates with the same frequency as the applied current as described by Ibl (14). Its magnitude is also

elated to the peak current density but reaches a limiting value governed by the diffusion coefficient of the ions involved. During the off time the concentration of the reactants build up again and if enough time is allocated will reach the equilibrium concentration of the bulk electrolyte. Typically for frequencies of several hundred cycles a second this diffusion distance is rather less than the corresponding diffusion distance for direct current deposition therefore it can be expected that the resulting morphologies of coatings under direct current deposition will be more dendritic or nodular than coatings formed under pulsed conditions. This is only a general description and a rigorous treatment of the problem would have to take into account the diffusion parameters of each ion separately as well as the mass transport conditions. If this diffusion distance is comparable to the dimension of the surface roughness then the asperities of the surface which protrude into the diffusion layer will be exposed to a concentration of the reactants which is higher than the average surface and therefore will experience a higher deposition rate. During pulsing however the average diffusion distance is usually small compared to the surface roughness so that the surface sees an uniform concentration of ions at even its rough places, then the deposition rate is everywhere about the same. It is for this reason that for pulsed current deposition a smoothing effect is often realized and dendrite formation is suppressed.

The effects of pulsed galvanostatic deposition on chromium content were determined as a function of current density for various duty cycles and are plotted in Fig. 7, for a fixed off

time of 2 ms. Generally as the current density increases so does the chromium content for all duty cycles from 20 to 90%. However the higher the duty cycle the higher the chromium content.There is a significant difference in the surface morphology of deposits produced by different waveforms as might be expected from Ibl's explanation of the deposition process. In Fig. 8a and 8b a comparison is made of surface morphology, using scanning electron microscopy, between a typical direct currrent deposit and a coating produced by pulsed current deposition. The surface of the direct deposit is clearly much rougher. The duty cycle also effects the surface roughness as is shown in Fig. 9a and Fig. 9b which illustrate two pulsed coatings produced under identical conditions except for duty cycle. As a general trend the smoother deposits are produced at lower duty cycles. The effect of on time for the same duty cycle is shown in Fig 10a and Fig. 10b, again the lower On time provides the smoother coating.

Cross section of a typical coating show that the deposit grows in a layered structure with the layers exhibiting marked chromium concentration gradients. The scanning electron micrograph shown in Fig. 11 is of a coating produced at a 33% duty cycle at 50 A/dm^2 and an On time of 0.2 ms. It was deposited on copper coated brass and etched in aqua regia.

PROPERTIES

Microhardness measurements have been made on several coatings as a function of duty cycles and are shown in Fig. 12, for current densities of 25 A/dm^2 and 50 a/dm^2. Both current density values result in a minimum microhardness at around 50%

duty cycle. As is shown below the chromium content generally increases with the duty cycles so that higher hardness alloys are also high in chromium content.

Data on corrosion performance can be obtained in a number of ways such as salt spray, potentiodynamic anodic polarization, current staircase, potentiostatic scratch, and other electrochemical test along with actual exposure to a corrosive environment for an extended time. For the time being the corrosion performance is being evaluated using the technique of potentiodynamic anodic polarization. This technique is covered by ASTM G5-78 (19) and is quite widely used by industry. Samples for the corrosion tests reported here were prepared on a rotating disc electrode made of brass which was plated with gold. We have also found that a nickel strike can form an excellent undercoat for the nickel chromium coatings. Corrosion results will only be reported for one alloy composition namely 18% Cr 82% Ni (Wt. %). This alloy composition is formed at Ø.1 ms On time and Ø.2 ms Off time at 5Ø A/dm^2 at 5ØØ rpm. The samples were about 1 cm. diameter. Results are given for both 1 N sulfuric acid and 3% sodium chloride electrolytes.

The corrosion data shown in Fig. 13, in sulfuric acid for nickel chromium is compared with data taken under similar conditions for 43Ø SS stainless steel. Note that the passive region extends to almost 1 volt SCE. When compared to 43ØSS stainless steel shown in Fig. 14, whose passive range is somewhat less it seems clear that this coating has a very strong tendency to passivate. In chloride environments the corrosion performance

is degraded significantly as shown in Fig. 15, compared with the performance of 430 stainless shown in Fig. 16.

The passive region is now only a few hundred millivolts however, the strong tendency of the current to drop upon reversal of the potential reveals an extreme resistance to pitting. A possible explanation for this excellent corrosion behavior lies in the particular microstructure of the coating. As in most binary alloys electrodeposited coatings, the second constituent is not uniformly distributed. Typically layers are formed that are rich in one of the constituents. This microstructure is typical for different coatings plated under the same conditions as was shown above. Clearly there are strong chromium concentration gradients present. It would seem reasonable to assume that corrosion would proceed into the coating until one of these layers was encountered and then spreads laterally until the outer layer was dissolved so that pitting is eliminated. Since the layer spacing is on the the order of 1 micron, in a 50 micron engineering coating more than 75 layers would have to be uniformly dissolved before that substrate could be attacked. This mechanism occurs in the duplex and triplex nickel systems used on automobile bumpers.

Two samples of nickel chromium coatings were studied by X-ray diffraction. The first is a direct current deposit designed to produce a 20% chromium content and the second is a pulsed deposit designed to produce a 6% chromium content. Neither of the coatings were examined directly for chromium content so that these studies need to be expanded upon. In the pulsed deposit

the Cr_3Ni and the CrNi phase were detected which for the direct current deposit only the Cr_3Ni phase seemed to be present. Both coatings contained metallic nickel. However, in the direct current deposit the nickel was extremely fine grained.

CONCLUSIONS

1. A process has been developed that is capable of producing thick coatings of nickel chromium alloy whose chromium content can be controlled through the deposition parameters in a range from about Ø.1 Wt. % chromium up to 6Ø Wt. % chromium.
2. The resultant coatings exhibit unusual corrosion resistant in both chloride and sulfuric acid environments. This behavior is thought to be a result of their unusual layered structure.
3. Microhardness measurements imply that the wear performance of these coatings should be excellent.
4. Distinct differences in surface morphology and in the types of crystal phases present has been observed between coatings produced by direct current deposition and by pulsed current deposition. The differences in surface morphology or roughness can be accounted for by Ibls theory describing the pulsating diffusion layer.

ACKNOWLEDGEMENTS

The author gratefully acknowledges the financial support of the American Electroplaters Society and Center for Materials Science of the National Bureau of Standards. The following students have worked on this project: Carlos Beauchamp, Ann Perry, and JoAnne Weinroth and their assistance along with that of Dr. Ilan Weisshaus has contributed a great deal to the success of this project.

REFERENCES

1. C. L. McBee and J. Kruger, Electrochem. Acta, 17,1337 (1972)

2. A.G. Revez and J. Kruger, Electrochem. Acta, 137
3. Forbes M. Miller and Nikolaja T. Bredza in Source Book on Materials Selection Vol.II ASM pub. pg 462, Metals Park Ohio, March 1977.
4. H. J. Grey, ASM News. Vol. 10, No. 12 Dec. 1979, pg.1
5. C.U. Chisom and R.J.G. Carnegie. Plating, 59, 28 Jan 1972
6. P. W. Stromatt, U.S.A. Patent 3,888,744 June 1975
7. T. Hayashi and A. Ishihama, Plating, 66 (1979) 36
8. A. Ishihama and T. Hayashi Personal *Communicatiion
9. M.A. Shluger and V.A. Kagakov. J. Phys. USSR 33 (1969) 101 and 33 (1960) 649
10. M. Gilshinski and J. Yahalom, J. Electrochem. Soc. 129,11 (1982) 2433
11. N.H. Dar, G. Ulrich and T. Schmidt. J. Chem. Soc. 111, 690 (1917) 707
12. S.D. Rasberry and F.J. Heinrich, Analytical Chem. 46,1 (1974)81
13. N. Ibl, J. Cl. Puippe and A. *Angerer, Surface Technology, 6(1978) 287
14. N. Ibl, Surface Technology 10 (1980) 81
15. K. Viswanathan, M.A.F. Epstein ad H. Y. Cheh, J. Electrochem. Soc. 125,11 (1978)
16. K. Viswanathan and H. Y. Cheh, J. Electrochem. Soc 125,10 (1978)
17. Proceedings, 1979 International Pulse Plating Symposium *Ap. 1979. Am Electroplaters Soc. Winter Park, Fla.
18. Proceedings, 1981 International Pulse Plating Symposium *Ap. 1981. Am. Electroplaters Soc. Winter Park, Fla.
19. ASTM G5-78, 1982, Am Society for Testing and Materials 1916 Race St., Philadelphia, Pa. 19103

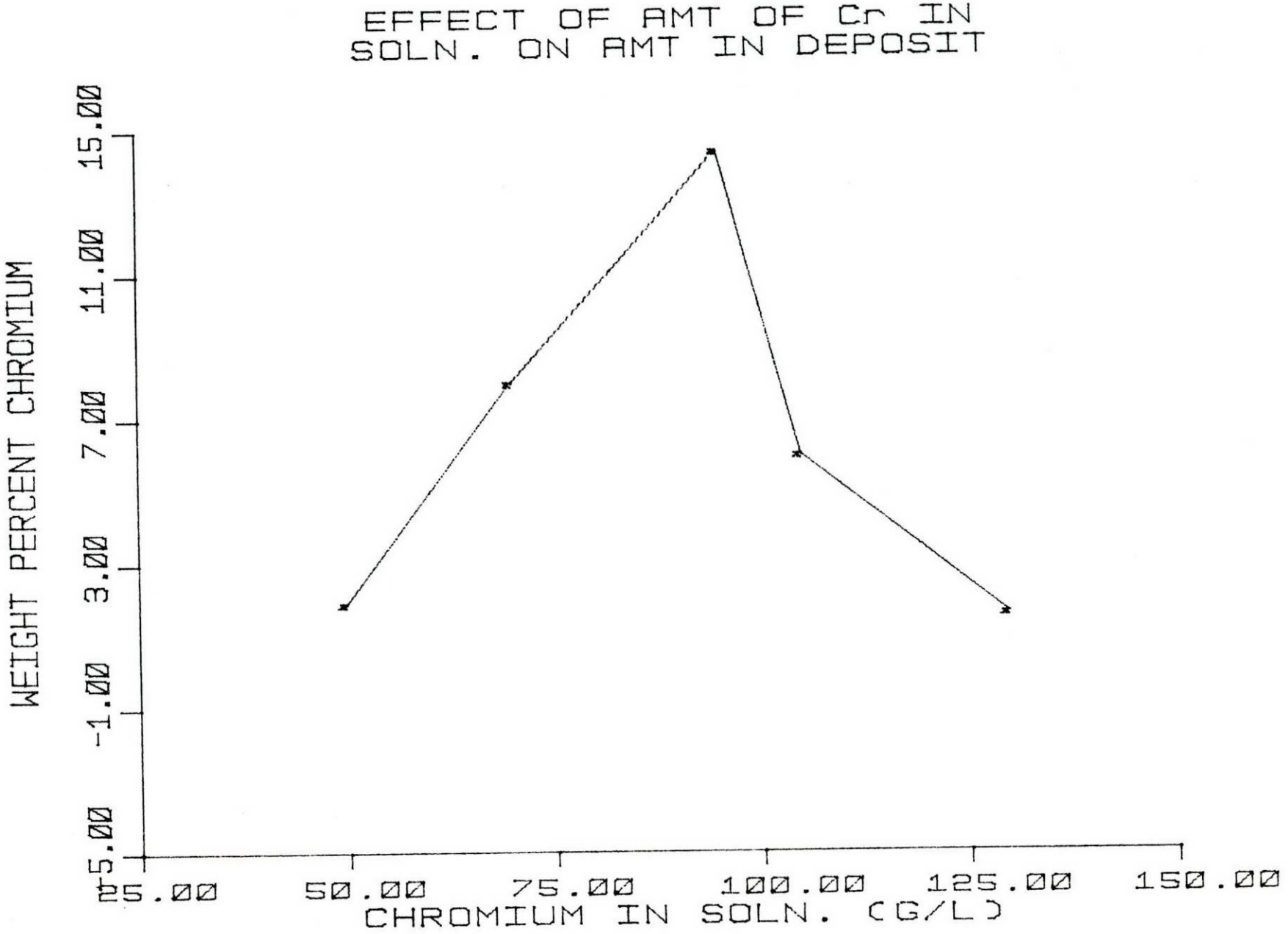

Fig. 1a. Variation of the Chromium content in the coating with chromium hexahydrate in the electrolyte.

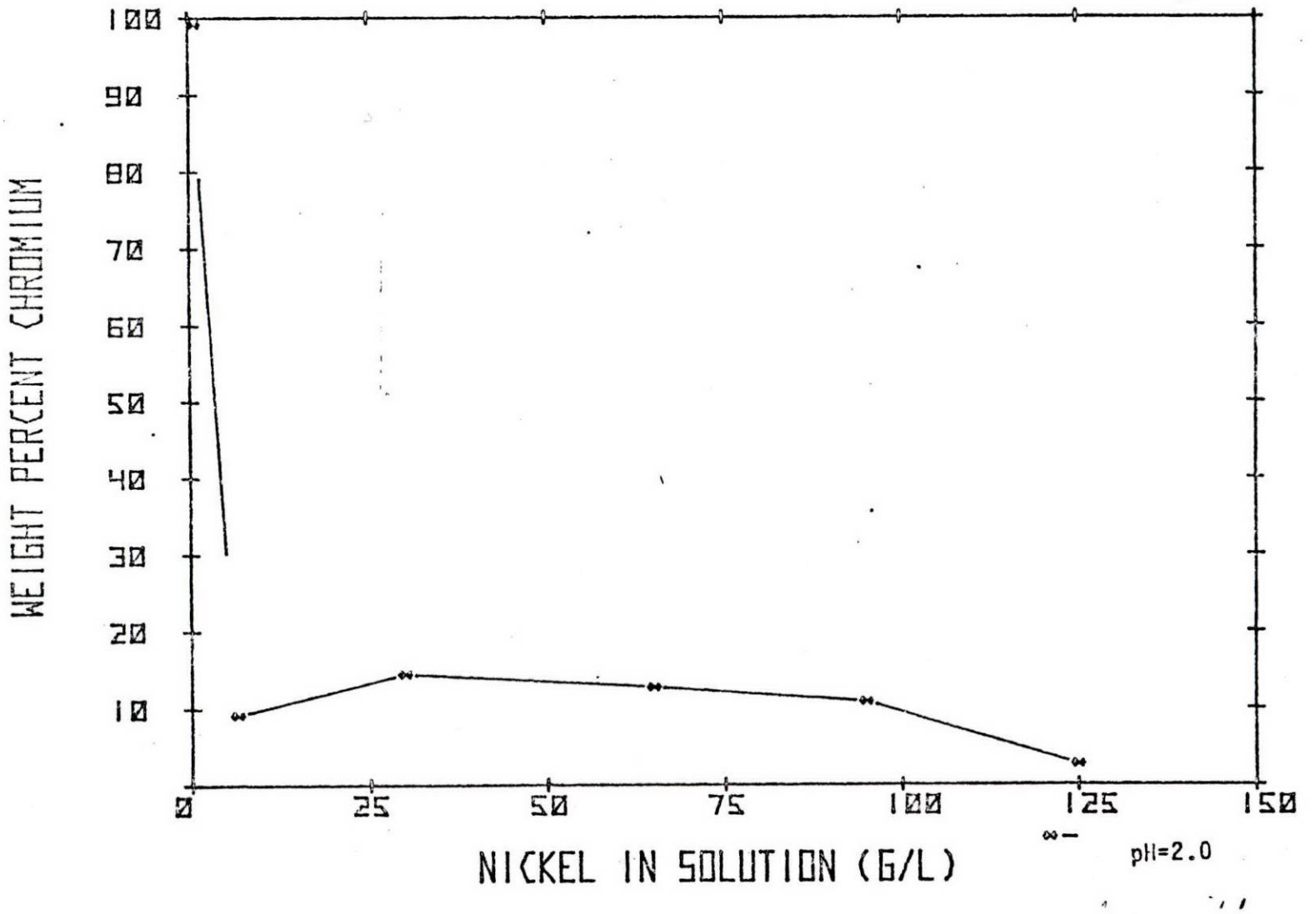

Fig. 1b. Variation of Chromium content in the coating with nickel hexahydrate in the electrolyte. (pH=2.0)

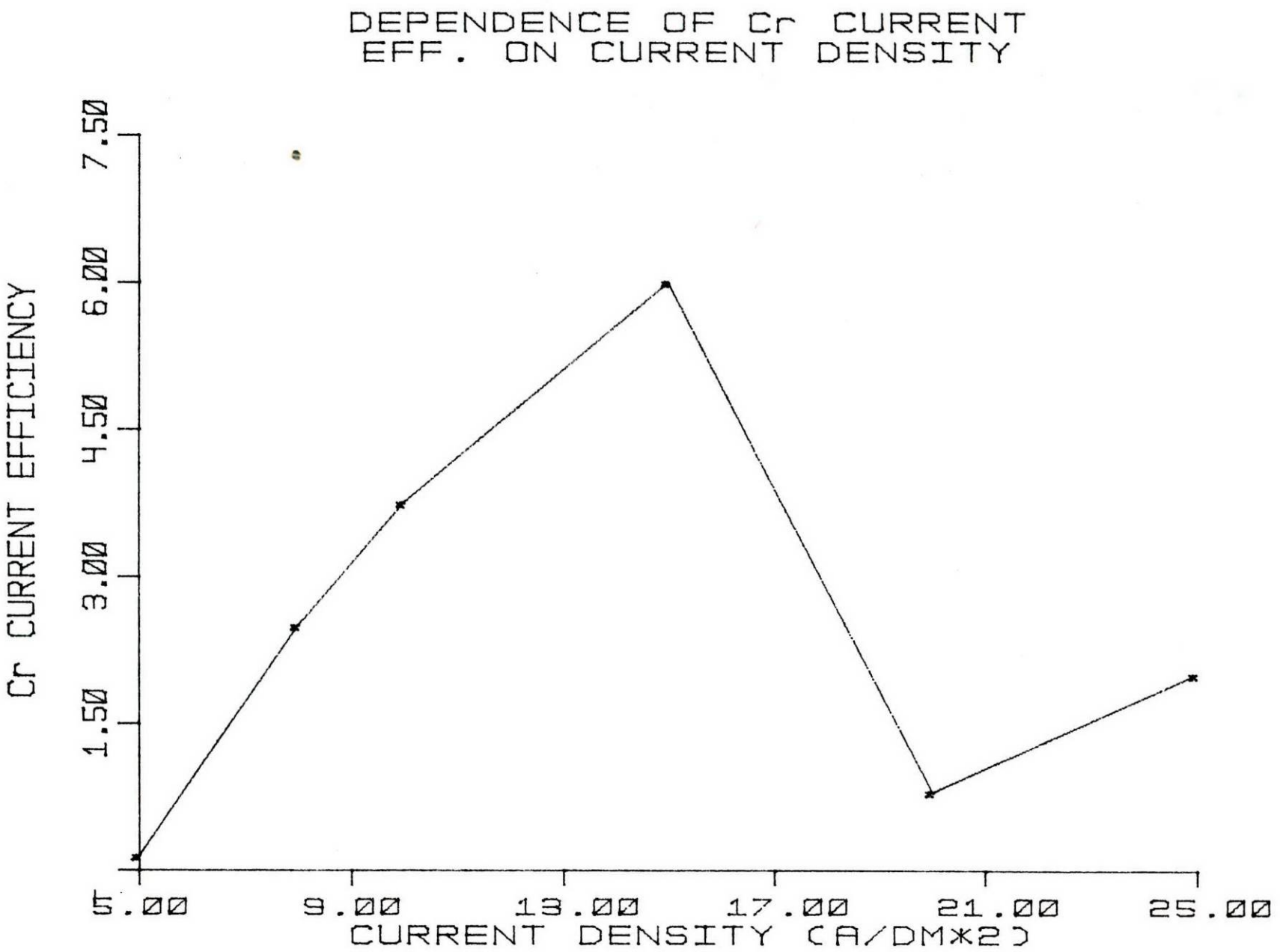

Fig. 2. Dependence of the current efficiency on the current density for the deposition of chromium only. (based on wt.% Cr. in alloy)

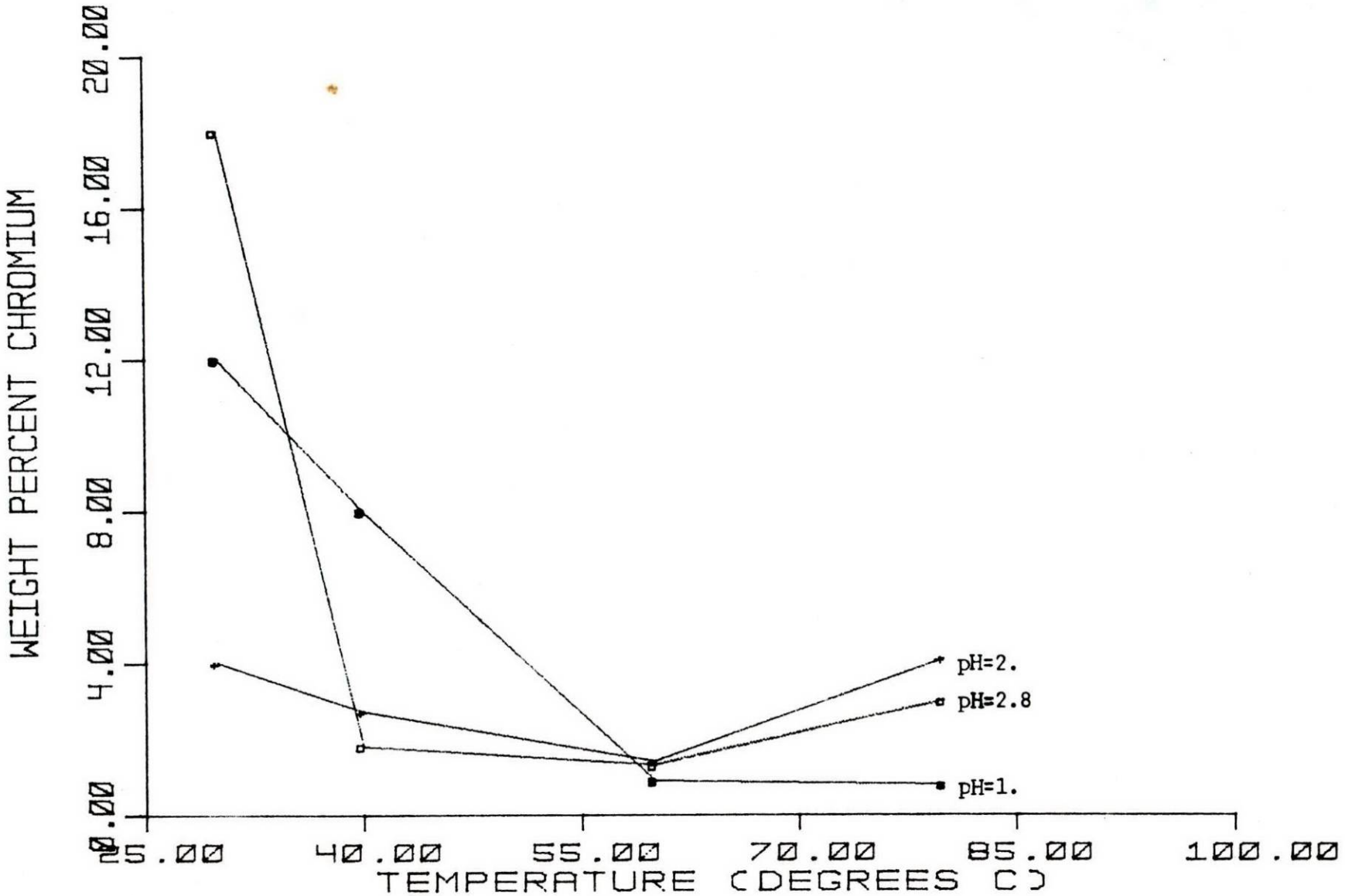

Fig. 3. Dependence of the chromium content of the alloy on the temperature and pH.

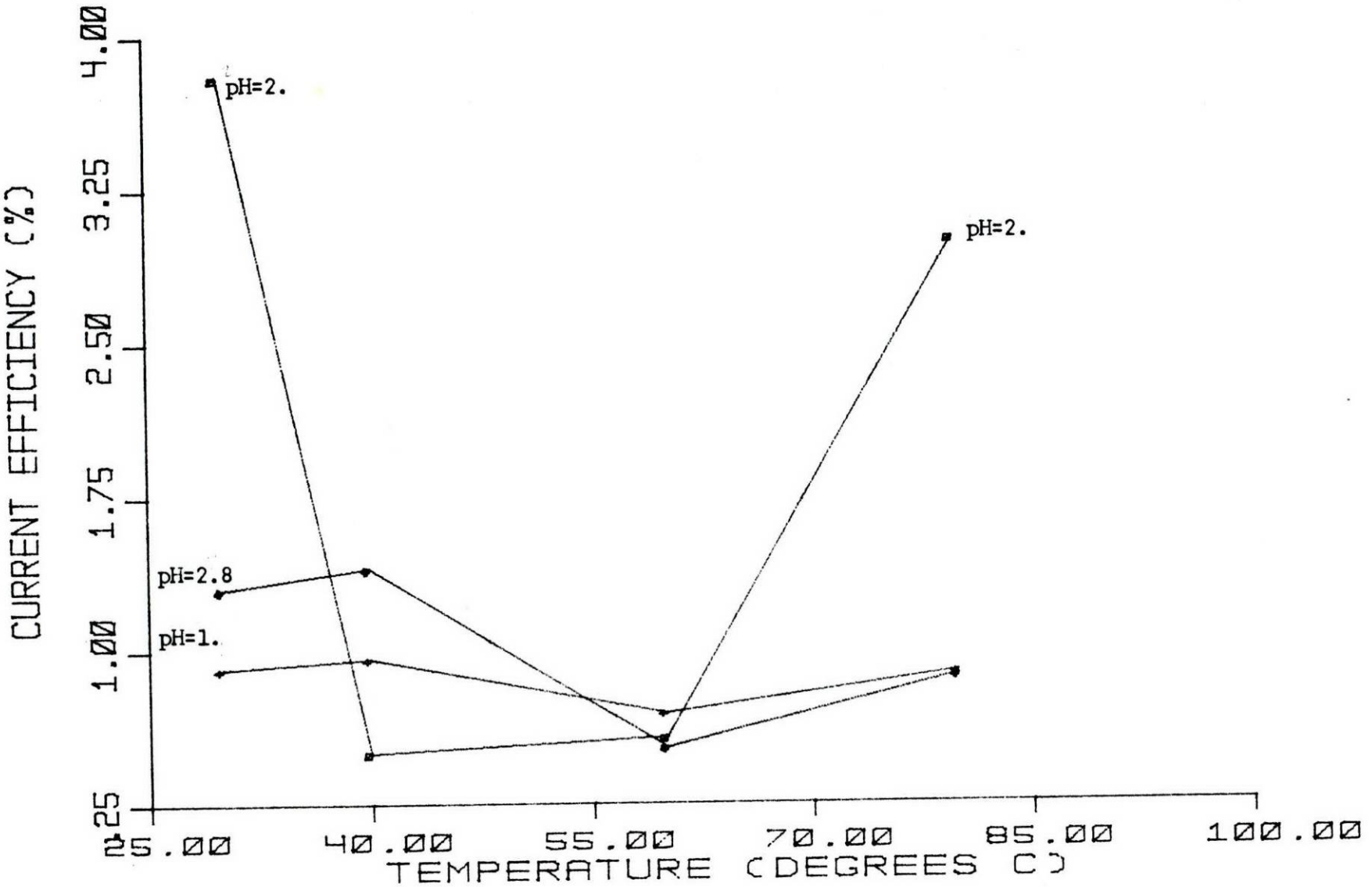

Fig. 4. Dependence of the chromium current efficiency on temperature of the electrolyte and on pH.

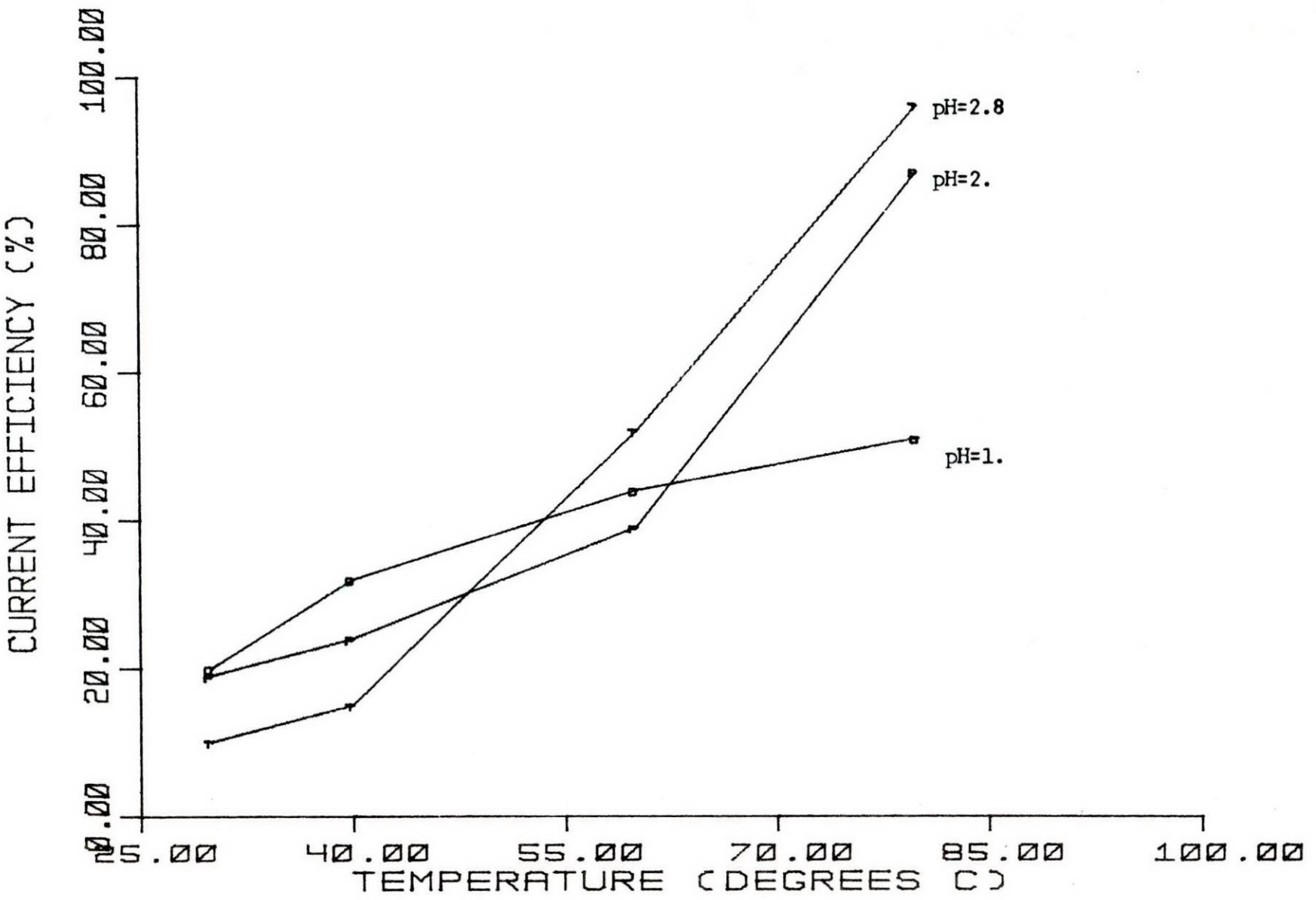

Fig. 5. The overall current efficiency as a function of temperature of the electrolyte and as a function of pH.

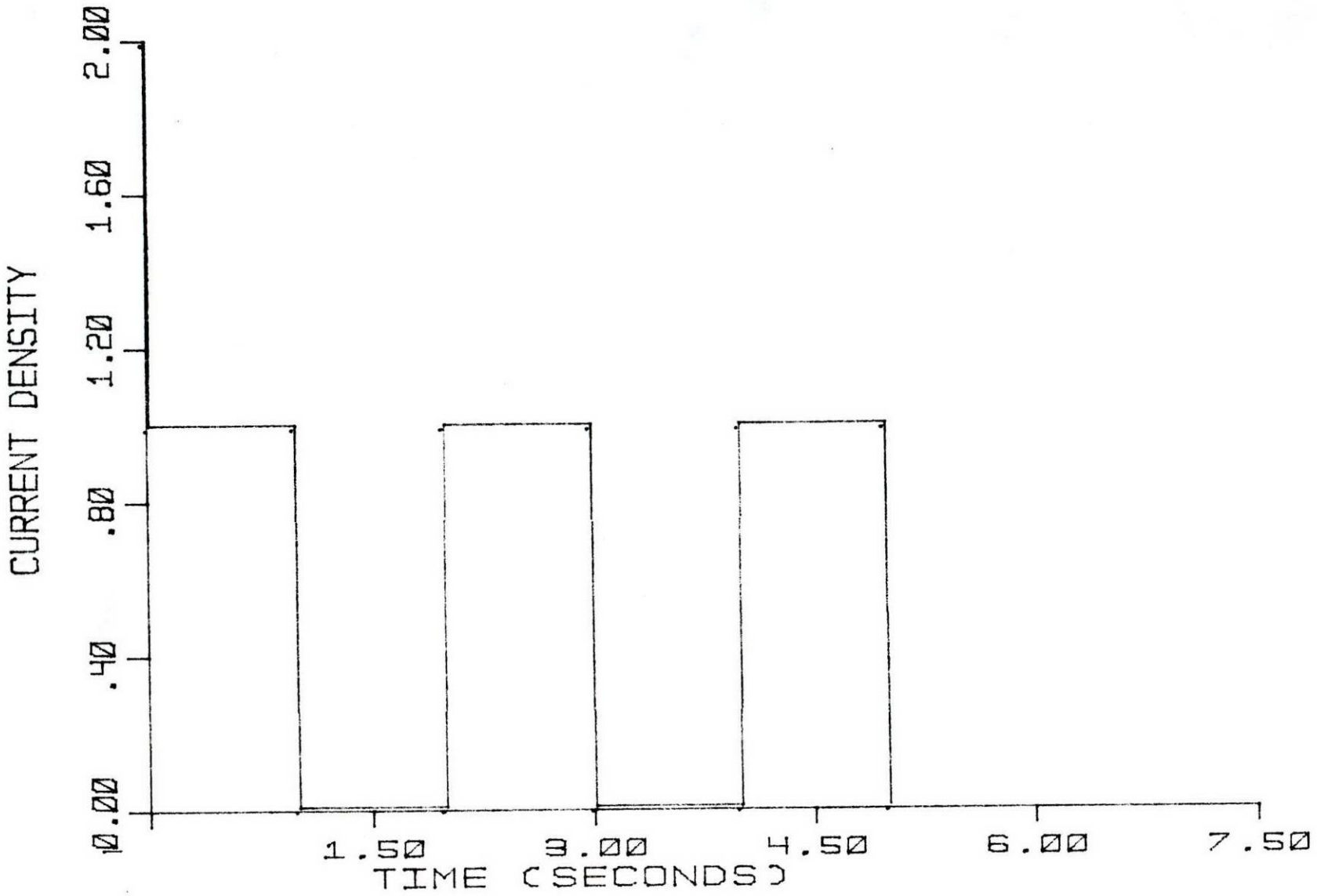

Fig. 6. Waveform of pulses used in galvanostatic deposition(arbitrary time scale)

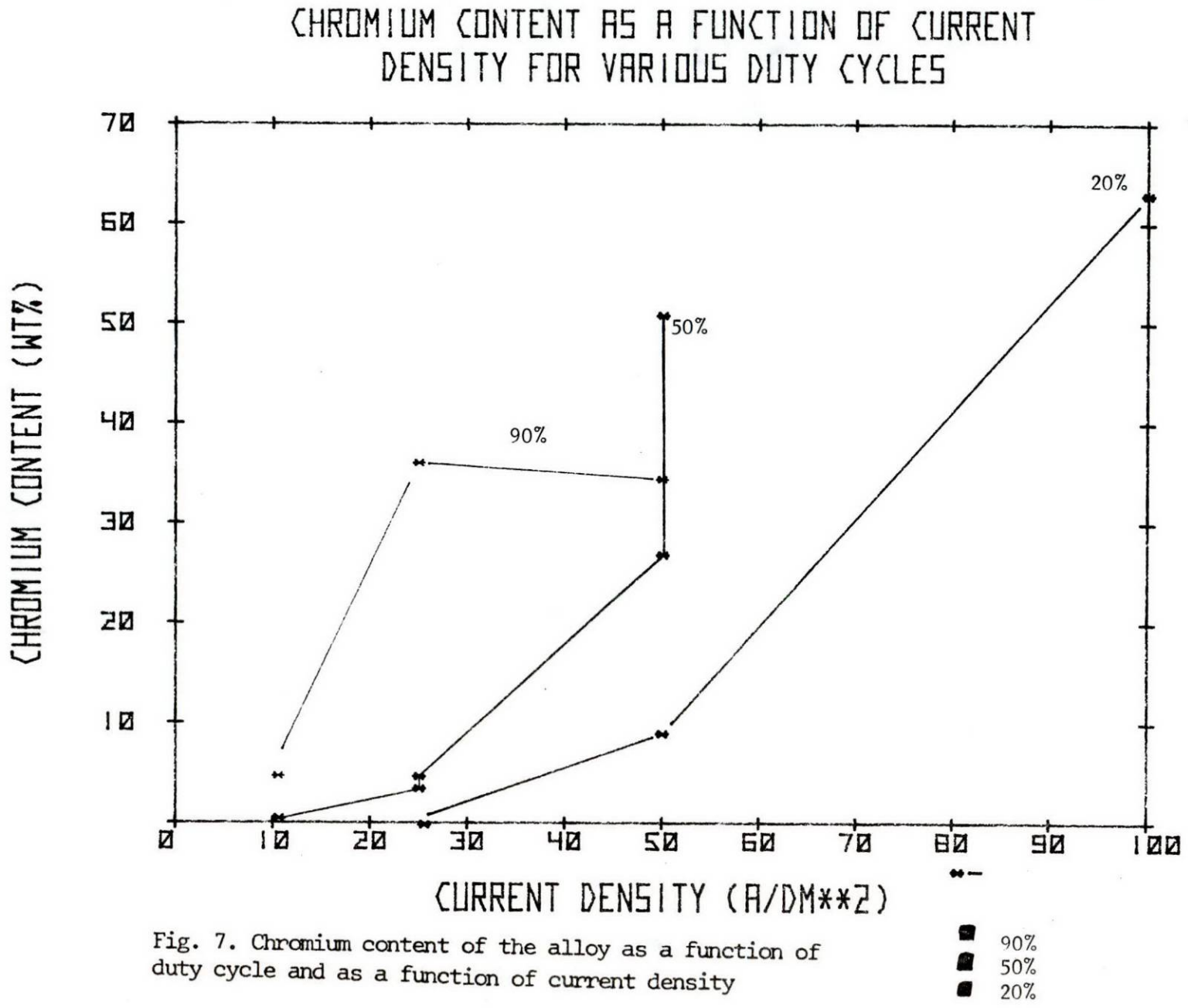

Fig. 7. Chromium content of the alloy as a function of duty cycle and as a function of current density

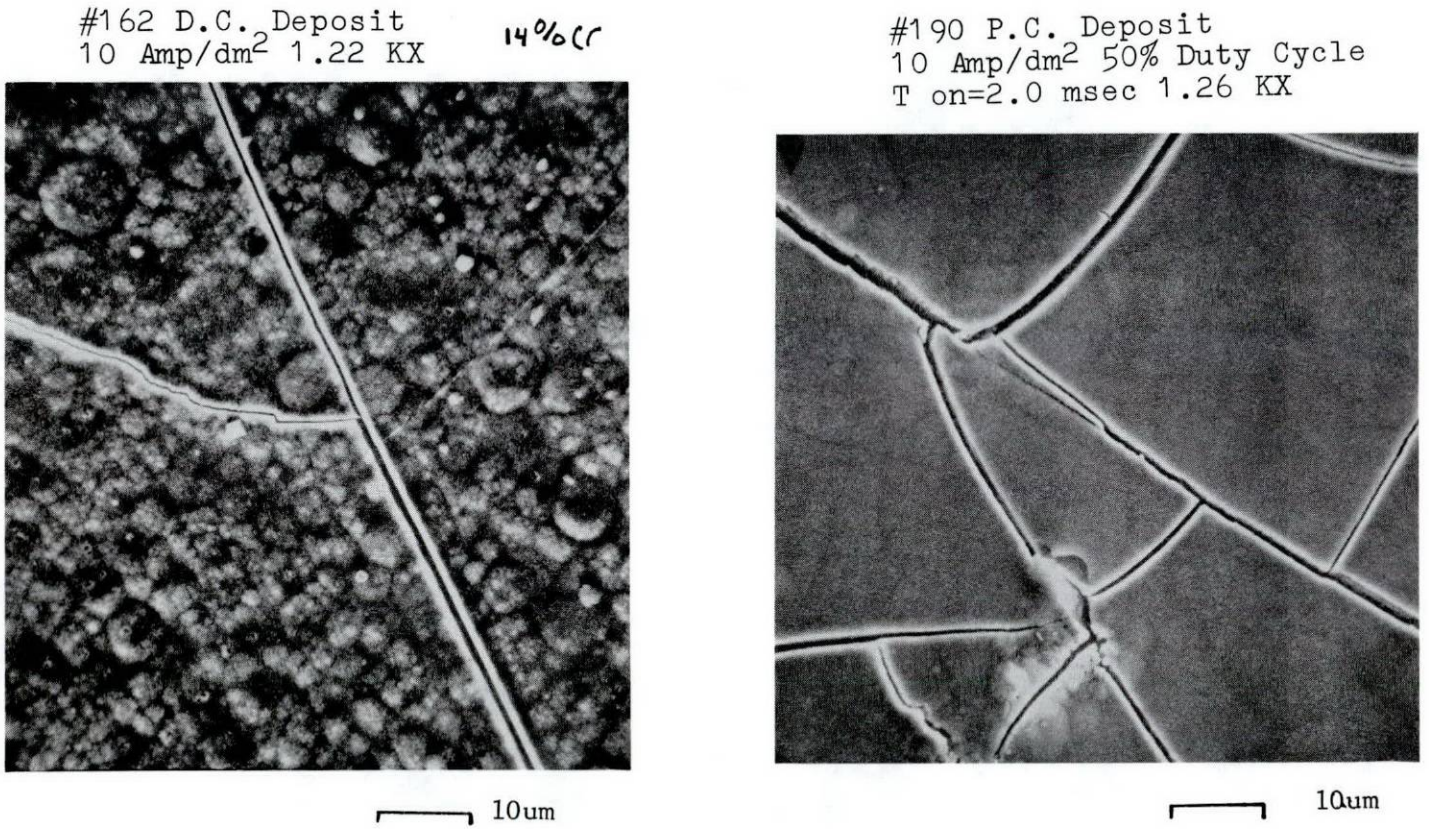

Figure 8. A comparison between direct current deposited alloy and pulsed deposited alloy under the same current density.

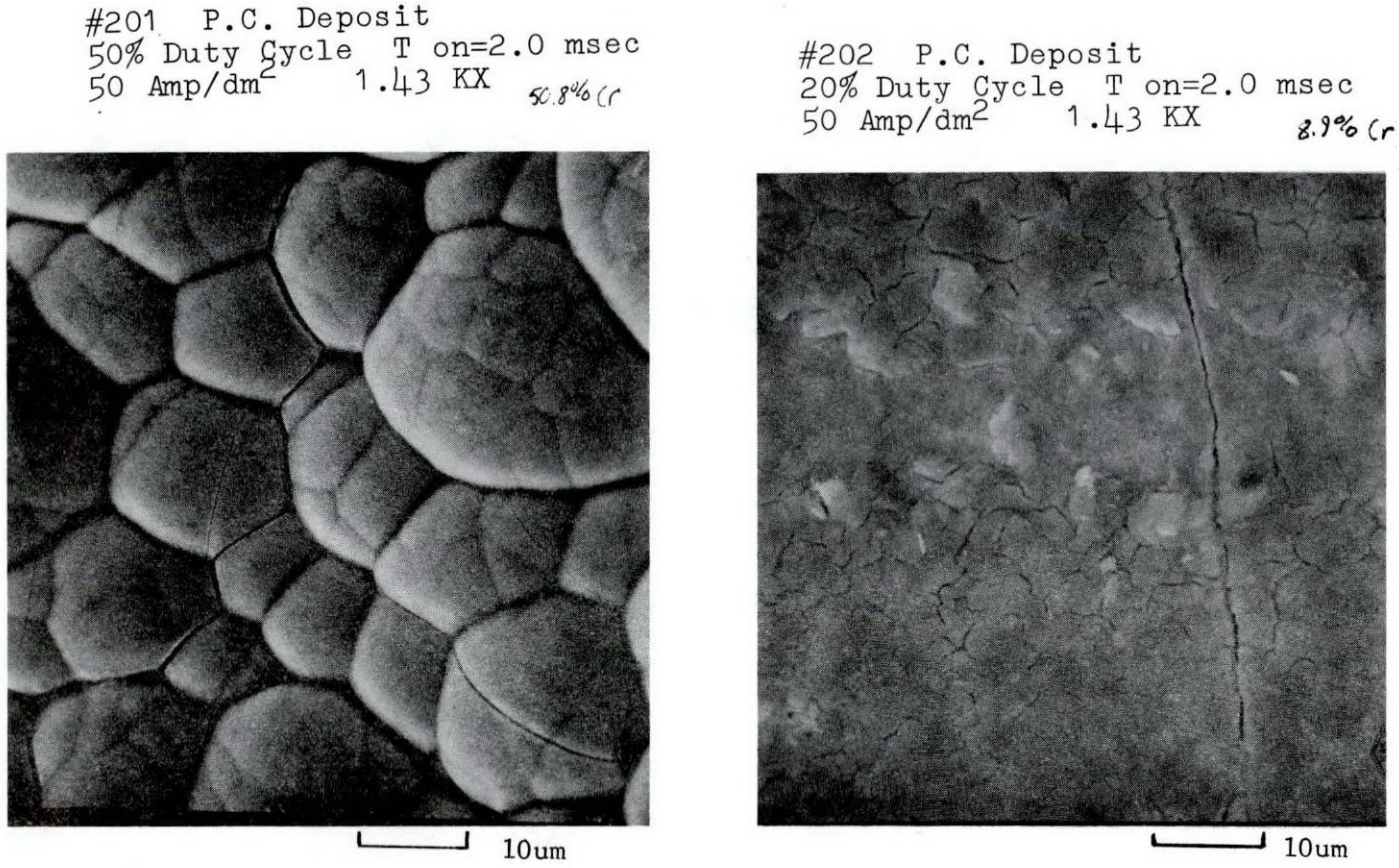

(a) (b)

Fig. 9. The effect of duty cycle on morphology.

#199 P.C. Deposit
25 Amp/dm^2 20% Duty Cycle
T on=2.0 msec 1.4 KX 1.9%Cr

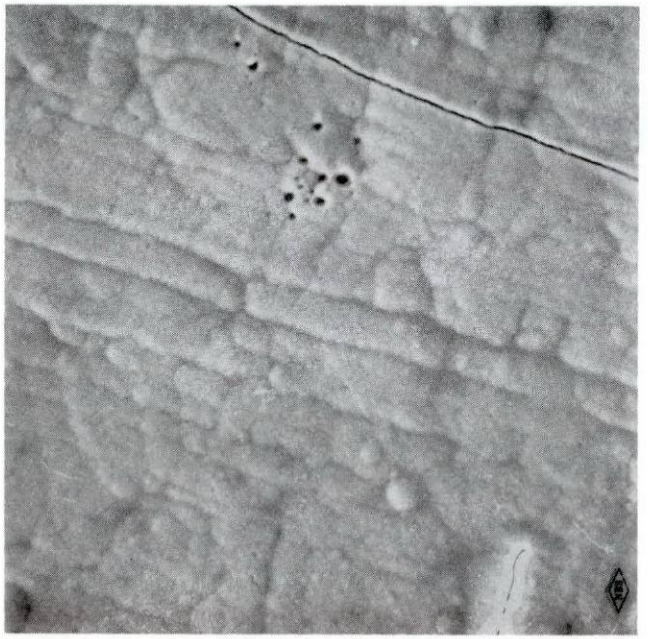

10um

(a)

#210 P.C. Deposit
20% Duty Cycle T on=1.0 msec
25 Amp/dm^2 1.38 KX

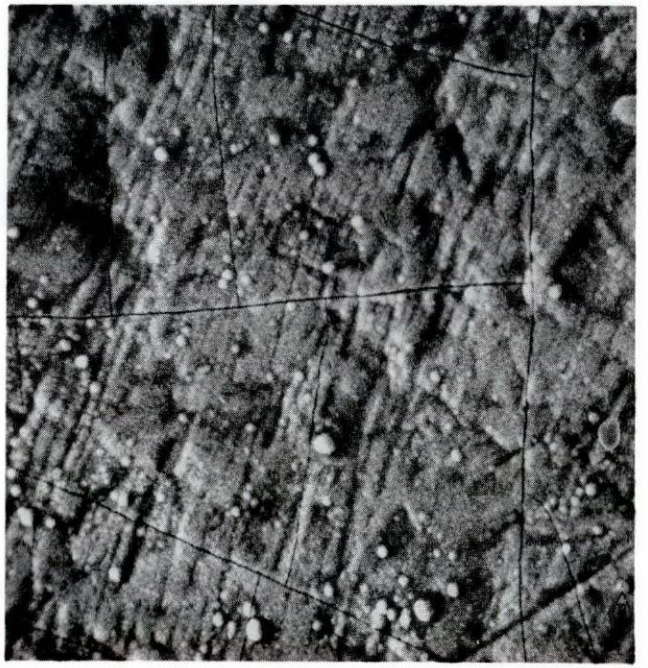

10um

(b)

Fig. 10. The effect on On time on the coating morphology. The duty cycle has been kept constant.

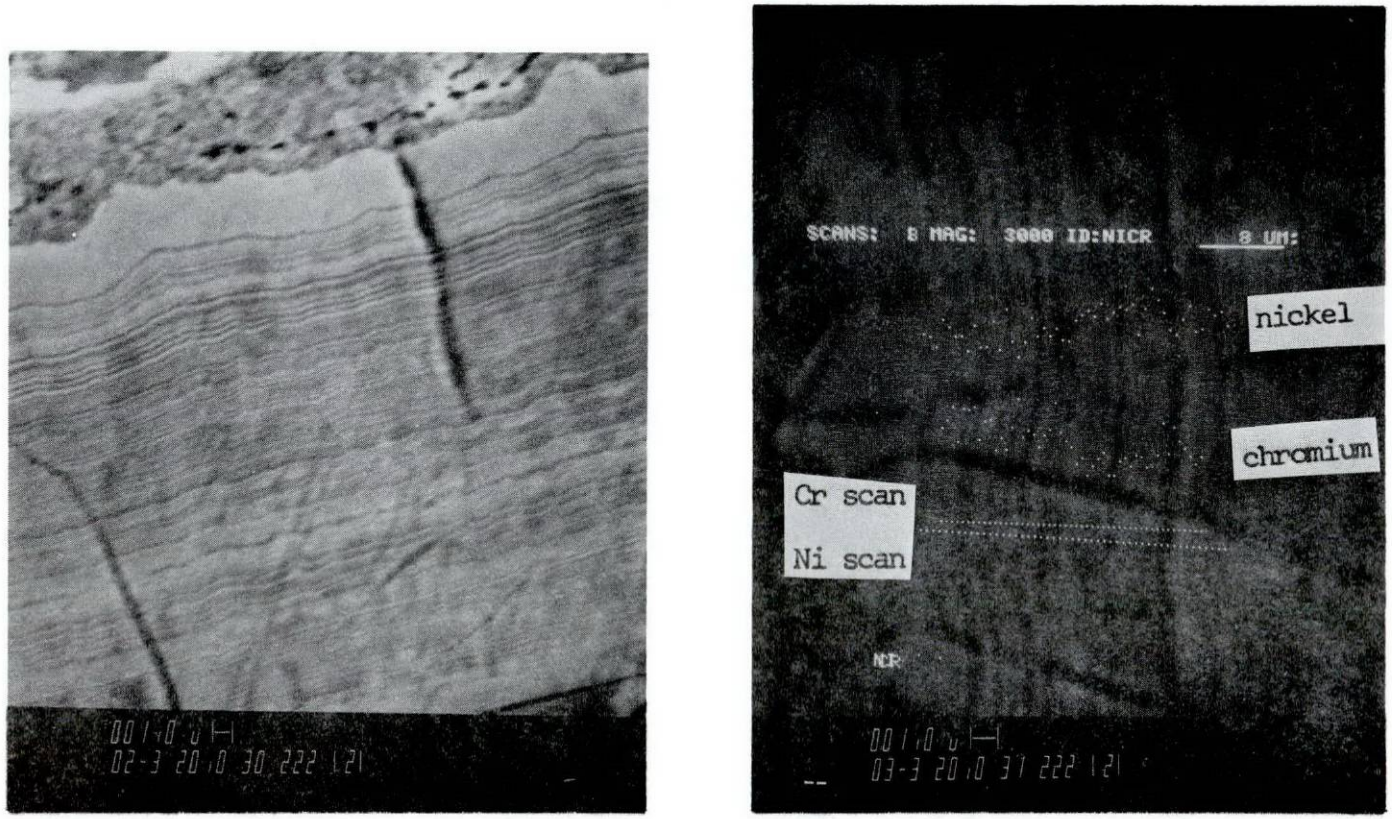

(a) (b)

Fig. 11. (a) SEM micrograph illustrating the laminated structure of a typical nickel-chromium alloy coating, (b) An X-ray line scan using Cr radiation illustrating that the periodic layer structure is a result of strong chromium concentration gradients. (sample etched in aqua regia)

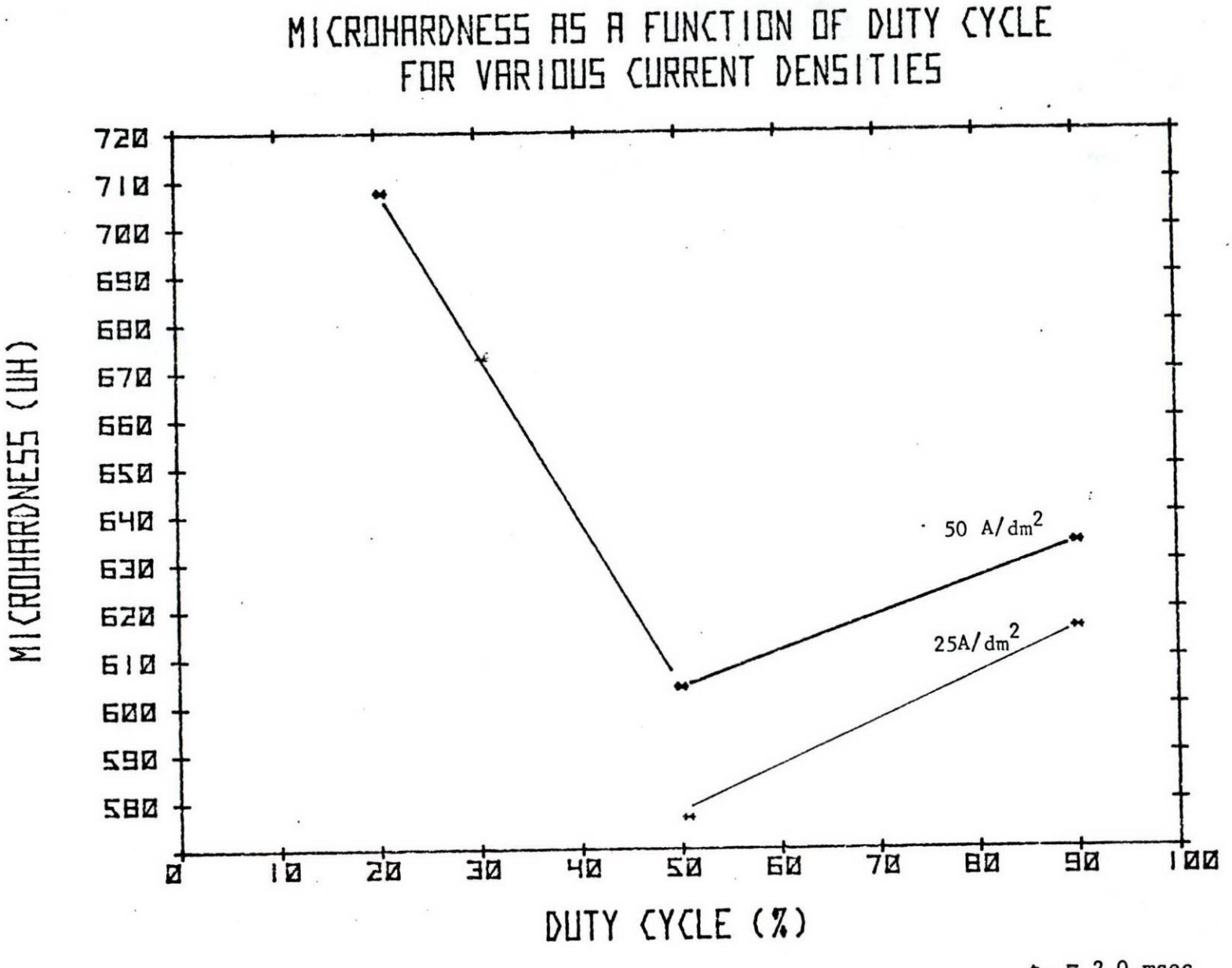

Fig. 12. Microhardness as a function of duty cycle for two different current densities.

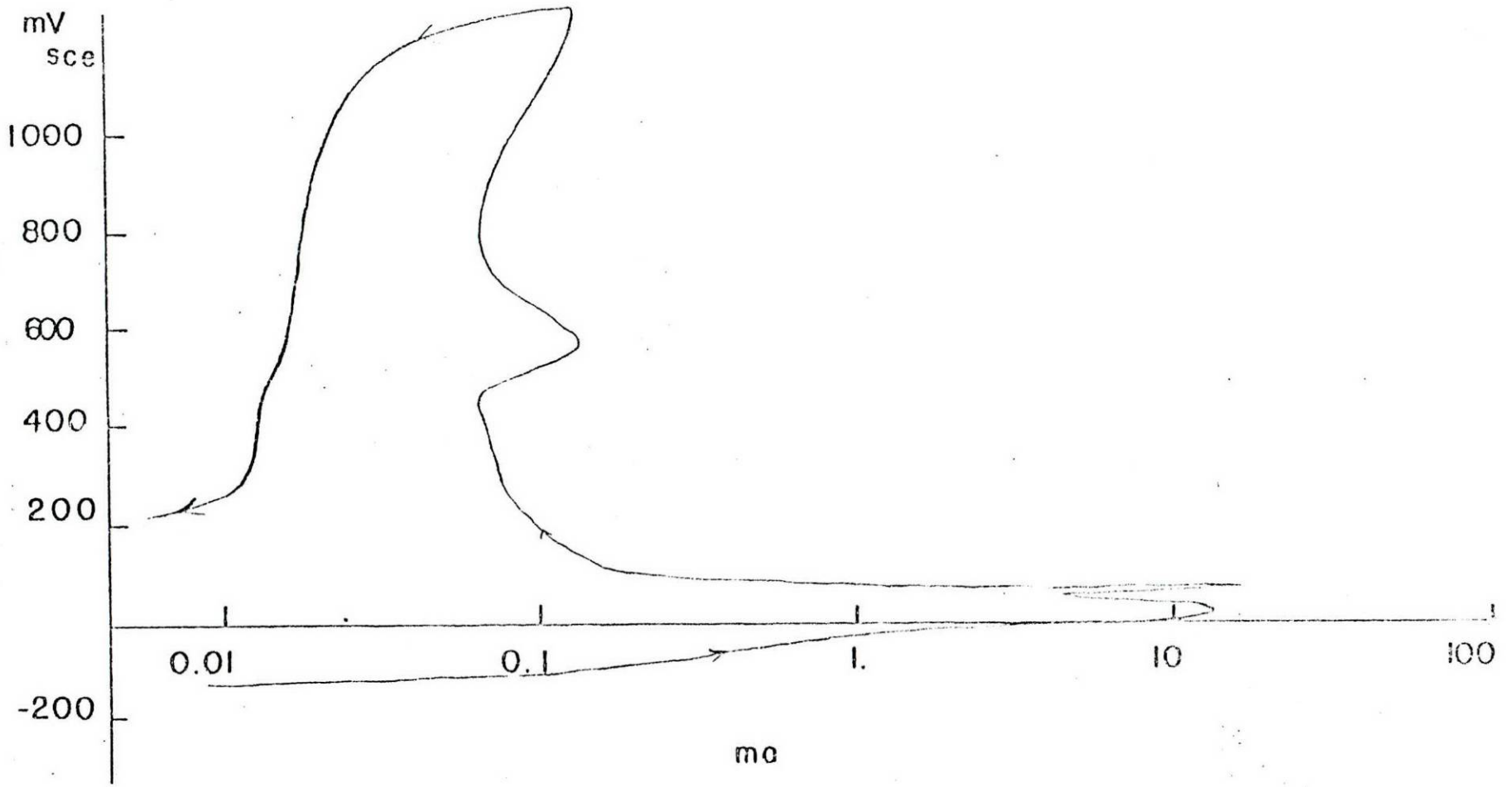

Fig. 13. Potentiodynamic anodic polarization data for a NiCr alloy (20% wt. Cr. nominal) in a 1N sulfuric acid electrolyte

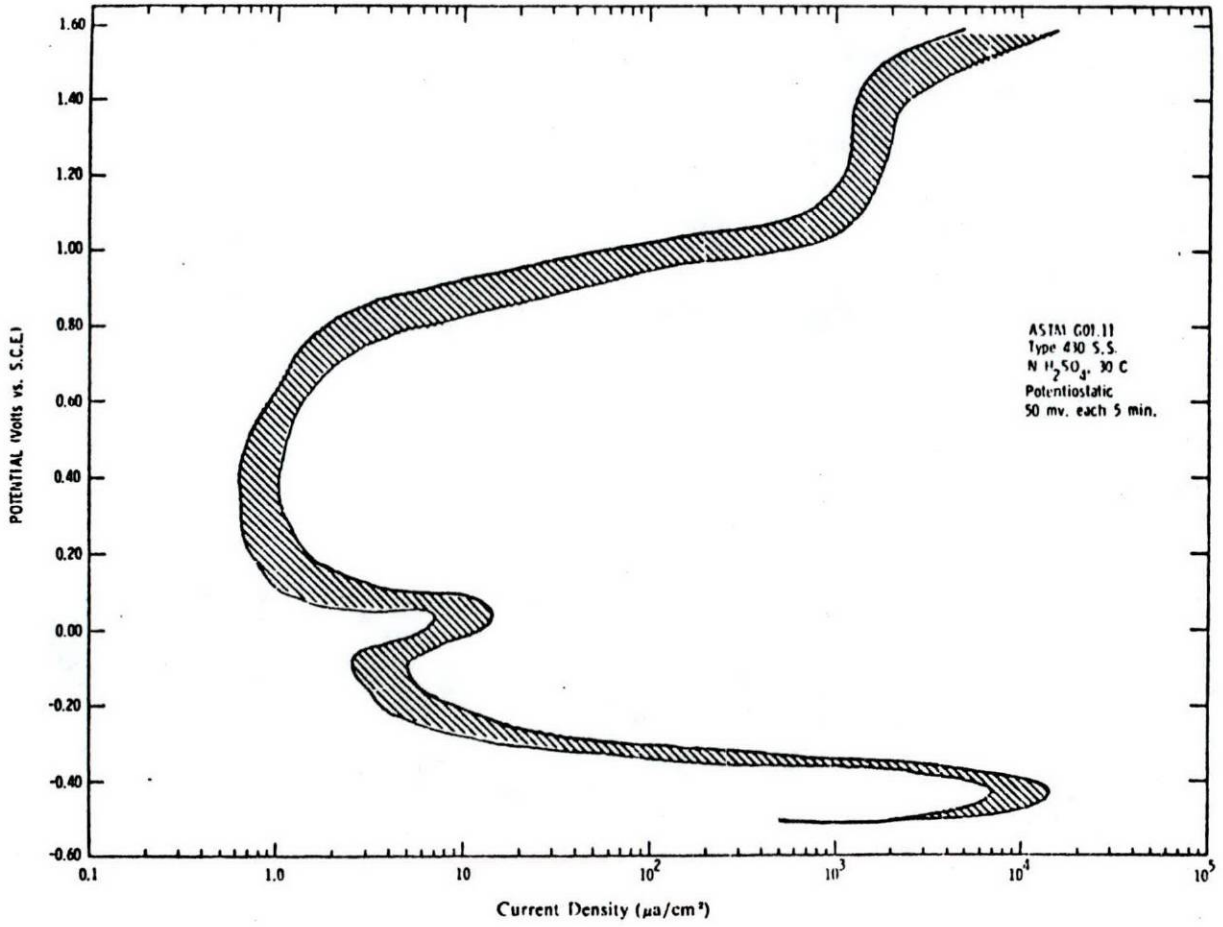

Fig. 14. Potentiodynamic anodic polarization data for 430 SS stainless steel (compare with Fig. 13 for NiCr)

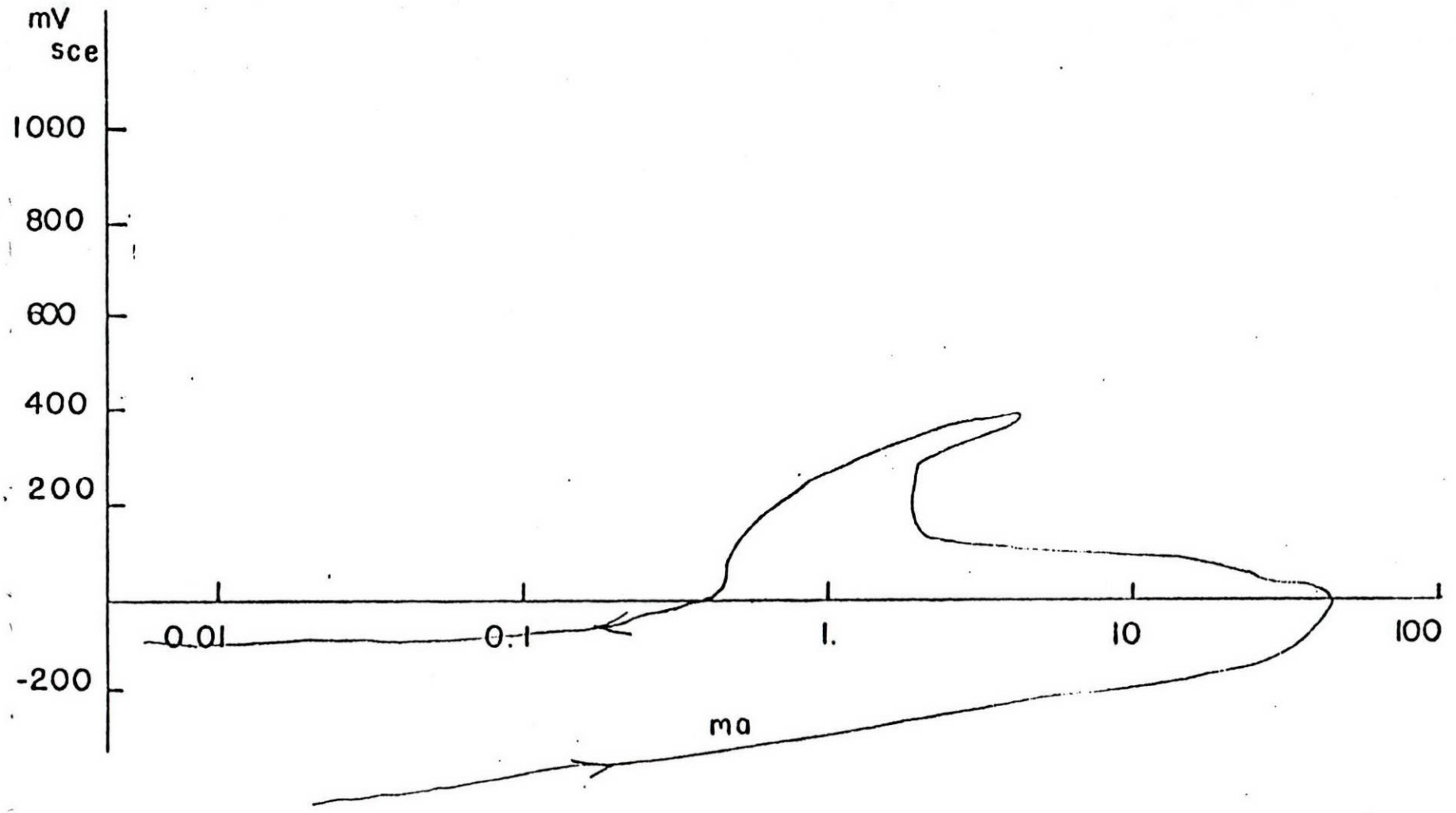

Fig. 15. Potentiodynamic anodic polarization data for a NiCr alloy coating (20 wt. % Cr nominal) in a 3 Wt. % sodium chloride electrolyte.

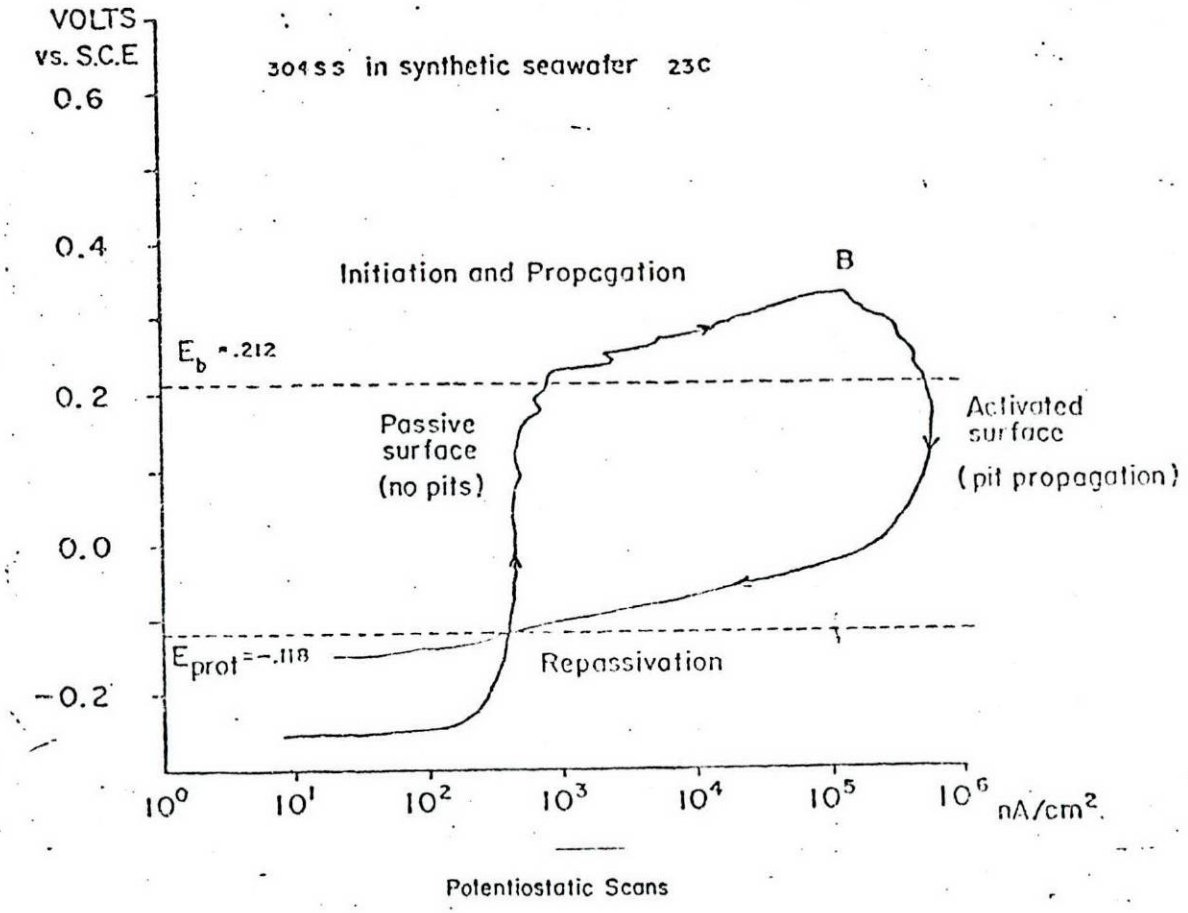

Fig. 16. Potentiodynamic anodic polarization data for 304 stainless steel in a 3 wt. % sodium chloride electrolyte.

A-3

Research Session A

Tensile Testing of Electrodeposits

M. Parente and Dr. Rolf Weil
Stevens Institute of Technology
Hoboken, NJ

strip chart. The tensile specimen, which is not shown, is held between screw grips (G). The separation of the grips, one of which is fixed and is also the one attached to the load cell, is measured by a linear variable differential transformer (LVDT). The output of the LVDT is also recorded on the strip chart. The strain rate can be varied by changing the motor speed and/or the specimen gage length.

As already mentioned, the preparation and mounting of the tensile specimen is very important for reliable results. Figure 2 shows the tensile specimen and the supporting frame, which serves to prevent deformation during mounting. Figure 2 is an enlargement. The actual specimen is only 1.3 cm long. Specimen preparation begins by placing a mask in the shape of the specimen and the supporting frame on the substrate. Using photoresist, the areas on the substrate not covered by the mask are insulated. The deposit thus will have the shape of the mask. For testing thin deposits, the supporting frame has to be strengthened. To accomplish the strengthening, the specimen gage length is covered with an insulating lacquer. After the proper activating treatment, a much heavier deposit is plated on the supporting frame and on the ends of the specimen where it will be gripped. The area plated with this reinforcing deposit was painted black for illustrative purposes and therefore appears darker in Figure 2A. Prior to testing, the substrate is dissolved. After mounting in the tensile machine, the frame is carefully cut. Figure 2B shows the specimen after testing and illustrates the absence of the supporting frame.

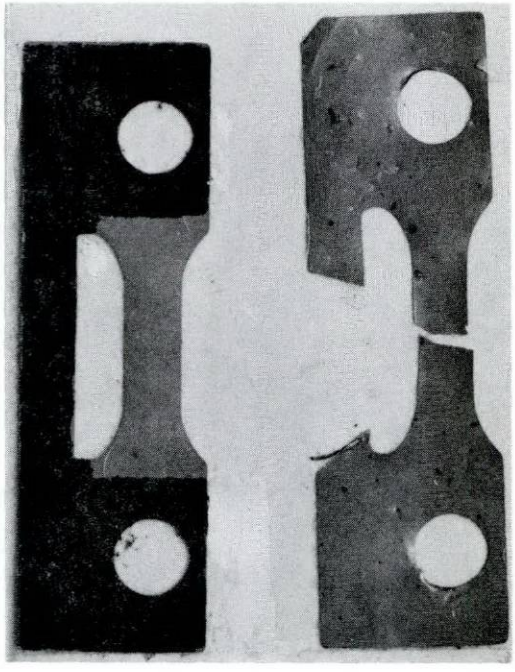

A B

Figure 2 Tensile Specimen

Some results have been obtained for nickel plated in an additive-free, all-sulfate solution on single-crystal and cube-textured copper substrates. A typical stress-strain graph, drawn by computer, is shown in Figure 3. The stress reaches a maximum value and then decreases again before fracture. This phenomenon, which is known as necking, results when there is a large decrease in the cross-sectional area over only a very small portion of the gage length. The actual strain in the necked region is quite large as evidenced by the reduction in the cross-sectional area at the fracture which was about 20% for the deposit depicted in Figure 3. The thickness of the deposit at the fracture, which is used to calculate the reduction in area, was determined by interferometry. All nickel deposits exhibited necking.

The significance of necking in practical plating lies in the application of the tensile-test results, which are obtained when the deposit is not attached to the substrate, to plated work pieces. Two conditions have to be

considered. One is the case when the whole piece, i.e., deposit and substrate, is subjected to the same load. The second case is when the stresses in the deposit and in the substrate are of opposite sign. The second case is encountered when the plated work piece is heated and then cooled and the deposit has a different coefficient of expansion from that of the substrate. This case is also found when the deposit is under internal stress as was discussed last year[1]. In the first case, a deposit showing the behavior depicted in Figure 3 would behave in a much more ductile fashion than the nominal tensile-test results indicate provided the substrate is also ductile. As the strain before fracture can approach the same value as the reduction in area, which as already indicated is quite large and probably greater than the elongation of the substrate, the deposit is unlikely to crack prematurely. In the second case, the large localized strain measured in the tensile test cannot be realized in the deposit. The substrate, which would deform only slightly, would not permit the deposit to deform appreciably either. However, in this case, it still would require a greater stress than the tensile strength to fracture the deposit.

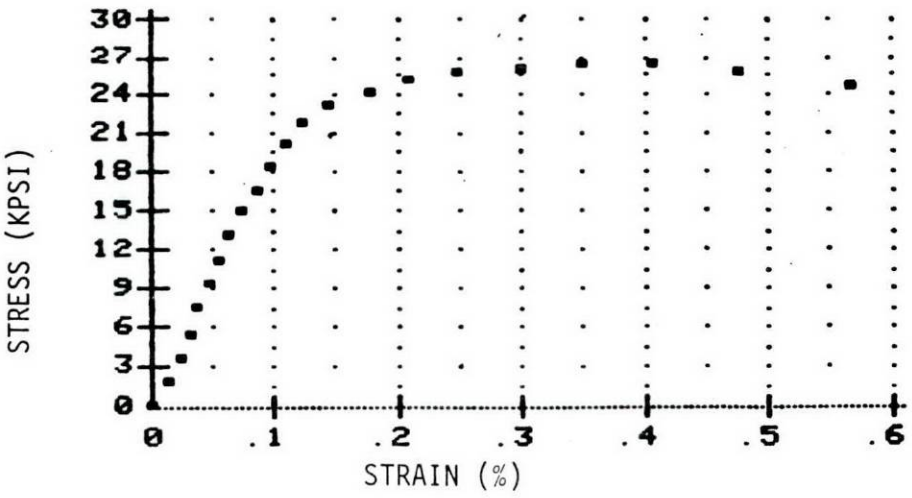

Figure 3 Computer-Drawn Stress-Strain Graph

It was also found that nickel plated epitaxially (i.e., it copies the substrate grain size and orientation) on cube-textured copper substrates had lower tensile strengths and elongations than those which were single crystals. The deposit the properties of which are depicted in Figure 3 was a single crystal and had a tensile strength of 184 MPa (~27,000 psi). Epitaxial deposits on a cube-textured substrate have tensile strengths of about 136 MPa (~20,000 psi). The difference can be attributed to a previously observed result[2] that the thickness of the deposit varies with grain orientation. The thickness of the single-crystal deposit is therefore more uniform while that of the one plated on the cube-textured substrate varies. The variation results because while most of the grains in a cube-textured substrate have the {100} crystal plane parallel to the surface, there are a number of grains with different orientations. In the case of nickel plated in an additive-free, all-sulfate solution, the thickest deposits grow on {100}-oriented substrate grains. On grains of other orientations, the deposit is thinner. This thickness variation can result in a deviation from a true uniaxial state of stress and a lower strength. When the deposit plated on cube-textured copper became nonepitaxial, i.e., it no longer copied the grain size and orientation of the substrate, a substantial strength increase resulted. A typical tensile-strength value was

306 MPa (~45,000 psi). The finer grain size and more uniform thickness are probably responsible for the higher strength.

The new tensile testing machine was also applied for the testing of electroless copper deposits used for printed-circuit boards. The widths and thicknesses of deposits on such boards are much smaller than those of the specimen which are generally tested to determine the mechanical properties. In the range of dimensions involved, there is a considerable effect of specimen size on the mechanical properties. With the new tensile machine it is possible to test specimens having the same dimensions as the deposits on printed-circuit boards. A paper dealing with this subject is being presented in the Electronics Session at this Conference.

References

1. M. Parente, J. J. Chiu and R. Weil, AES, 69th Annual Technical Conference, Session C.

2. H. J. Choi and R. Weil, Plating and Surface Finishing, 68, 110 (May 1981).

3. M. Parente, R. Weil and M. Paunovic, AES, 70th Annual Conference, Electronics Session

A-4

Research Session A

Hazardous Sludge Reduction

Lt. James R. Aldrich, USAF
Tyndall AFB, FL
Charles G. Roberts and Edward D. Handel
Centec Corp.
Reston, VA

HAZARDOUS SLUDGE REDUCTION

by

LT James R. Aldrich
United States Air Force
Tyndall AFB, Florida

Charles G. Roberts
CENTEC Corporation
11260 Roger Bacon Drive
Reston, Virginia

Edward D. Handel
CENTEC Corporation

FOREWORD

Stated simply, the Air Force Mission is to "Fly and Fight." As a result, we have over 70 different types of aircraft, ranging from the huge C-5A Galaxy to the relatively small T-33 trainers. These aircraft all have one common factor--they all need preventive maintenance. An integral part of this maintenance is the periodic rework of components, engines, air frames, landing gear, etc. To accomplish this mission, the Air Force has five major Air Logistic Centers (AFLCs) under the Air Force Logistics Command. These maintenance centers, located in Texas, Georgia, California, Oklahoma, and Utah, split the major maintenance duties by both geographic location of the aircraft homebase and by specific maintenance operation. All maintenance centers, however, have extensive electroplating capabilities for chromium, cadmium, nickel, and copper. Although some precious metal plating is also done, in comparison to the above metals, it is insignificant.

Under the Resource Conservation and Recovery Act (RCRA) Hazardous Waste and Consolidated Permit Regulations, the wastes generated by these electroplating facilities are classified as hazardous. Because wastes from these shops are channeled through Industrial Waste Treatment Plants (IWTPs) the resulting sludges also become hazardous and require special handling and disposal methods. Presently, most hazardous sludge is disposed

of in landfills; however, the costs have risen from $8 to $15 per ton before RCRA to $100 per ton and they are expected to rise even further.

Given the present configuration of the treatment facilities, available funding, and the lead time required for major construction, an interim solution to the problems of sludge volume and disposal costs had to be found. This is not to say that the Air Force is not keenly aware of its public responsibility in the hazardous waste area. Indeed, other research projects are aimed specifically at eliminating waste through reuse and recycling. The fact remains that hazardous sludge is a problem today and, under present constraints, an intermediate or "tide-us-over" step had to be taken.

With that in mind, a research project was begun with three objectives as follows:

1. Reduce the volume of hazardous sludge generated at the Air Force IWTPs.

2. Make the resulting sludge "non-hazardous" under the Environmental Protection Agency's criteria.

3. Accomplish the above with a minimum of changes in equipment and procedures at the plating shops and the IWTPs.

Meeting these three objectives could save the Air Force a considerable sum of money, get the treatment equipment on line quickly, and buy the time needed for the long-term recycling research.

The following report contains the results of the testing procedures and a summary of the reseach results.

OVERVIEW

The hazardous constituents in the treatment sludges often leach when exposed to the aqueous, acidic environment common to many sanitary landfills. To determine the leachability of hazardous wastes, EPA has adopted a test procedure that simulates this acidic condition. The test is referred to as the Extraction Procedure (EP). A measured sample of the sludge is placed in distilled water, a fixed amount of acid is added, and the mixture is agitated for 24 hours. The aqueous portion of the mixture is then analyzed for the presence of toxic constituents to determine to what extent they leached from the sludge. By comparing the results of the analysis to the maximum allowable concentrations, shown in Table 1, a level of toxicity can be determined. If the EP test results show that a given sludge consistently leaches less than the EPA standards, with a reasonable margin of safety, the sludge may be reclassified as nonhazardous. This reclassification would allow the generator to dispose of the waste by less expensive nonhazardous waste methods. EPA has established a "delisting" procedure for generators of hazardous sludges to petition for the reclassified status.

TABLE 1

EPA STANDARDS FOR LEACHABILITY

OF SLUDGES UNDER THE EP TEST[a]

Contaminant	Maximum Concentration (mg/liter)
Arsenic	5.0
Barium	100.0
Cadmium	1.0
Chromium	5.0
Lead	5.0
Mercury	0.2
Selenium	1.0
Silver	5.0

[a]U.S. Environmental Protection Agency, Federal Register, V. 45, No. 98:33122, May 14, 1980.

The results from the leaching tests on electroplating sludges are highly variable, depending on the types and concentrations of metals in the sludge, the amount of free and interstitial wastewater present in the sludge, and the final pH of the aqueous solution. Some electroplating treatment sludges readily pass the EP test while others fail due to high leaching of one or more metals. The sludge samples from the ALCs have shown a tendency to fail the leaching test for chromium and cadmium making their delisting impossible at this time.

This experimental research project was designed specifically to help the Air Force reduce the quantities of hazardous sludge produced by treatment of their mixed metal wastewaters, then treat the toxic metal sludges to allow delisting and ultimate disposal via methods approved for nonhazardous wastes. Because disposal costs are often a function of waste volume, the goal of minimizing the sludge volume could greatly reduce the overall cost of waste treatment.

This project consisted of five tasks and was conducted over a 2-year period. While this paper focuses on the two experimental phases, all five tasks are described briefly to illustrate the scope of the project.

Task I: A comprehensive literature search was conducted to establish the current state of technology for the removal of dissolved metals from industrial wastestreams and for the separation of heavy metals from mixed-metal sludges.

Task II: The EP test was used to characterize sludges generated at Air Force IWTPs to obtain baseline data on the hazardous nature of these sludges.

Task III: This experimental oriented task involved laboratory-scale testing of selected processes designed to reduce the dry weight of solids generated during the metal precipitation process.

Task IV: This task, also experimental in nature, involved the development of sludge treatment techniques to reduce the leachability of toxic metals to a level that would qualify the sludges for delisting. In addition, an effort was made to investigate methods of metal separation and recovery.

Task V: Basic design and cost data are currently being developed for a prototype system employing the most promising techniques from Tasks III and IV.

As developed, completion of these tasks would fulfill three objectives. First, as previously mentioned, the main focus was placed on end-of-pipe treatment processes that would be simpler

and quicker to put on line. Next, the criteria for selection of the final treatment process were to include capital costs, operating costs, metal removal efficiency, and complexity of operation, with the greatest emphasis on the dry weight of both hazardous and nonhazardous sludges. Finally, the sludge produced would be required to leach less than one-third the level deemed hazardous by EPA. This constraint was selected because delisting petitions are decided on a case-by-case basis. Previous contact with EPA had revealed that a sludge would generally have to demonstrate this low level of leaching to receive approval for delisting.

Experimental Study of Metal Removal Technologies

Hydroxide precipitation using lime for pH adjustment was identified in Task I as the "conventional treatment technology" to remove metals from mixed metal wastestreams. This treatment method was therefore selected as the control for evaluation of all other tested technologies. Metal removal processes identified in the literature search with the potential for producing a reduced quantity of sludge were selected for screening tests. The potential processes were evaluated using a computerized worth assessment model designed to provide an objective ranking based on a list of input characteristics. The following processes were selected for the Task III experimental screening studies:

1. Lime treatment - To provide baseline data.

2. Caustic treatment - Hydroxide precipitation using caustic in place of lime for pH adjustment to study the effect of pH reagent on sludge generation.

3. Water softening - Since water hardness varies by location, the effect of water softening on sludge generation was investigated.

4. Segretated treatment of hexavalent chromium - This treatment step was studied to determine the effect of segregated treatment on sludge generation.

5. Treatment chemicals for the reduction of hexavalent chromium - Since ferrous sulfate and sodium bisulfite are commonly used, a comparison of sludge generation was done.

6. Combined oxide precipitation and cyanide oxidation - This treatment technology uses a strong oxidizing agent such as ozone to treat cyanide and produce a sludge mixture of metal oxides and metal hydroxides. Although ozone was reportedly used to condition the precipitate following the pH adjustment of mixed metal wastewaters

with lime in the Ozodyne process, the use of a strong oxidizing agent to carry out the actual precipitation had not been performed.

7. Sodium borohydride (SBH) treatment - Although the literature indicated SBH could precipitate single or dual metal waste streams, treatment of complex metal waste streams and sludge generation were investigated.

The screening tests demonstrated that lime treatment produced 945 mg of sludge per liter of contrived wastewater.[1] The composition of all the contrived wastewaters used in this project are presented in Tables 2 through 5. This sludge was observed to settle well.

TABLE 2

COMPOSITION OF CONTRIVED WASTEWATER #1 (WW#1)

For Task III Screening Tests

Constituent	Concentration, mg/l	Chemical Used
Cr^{+6}	15	CrO_3
Cr^{+3}	30	$Cr(NO_3)_3 \cdot 9H_2O$
Cd^{+2}	1	$Cd(NO_3)_2 \cdot 4H_2O$
Cu^{+2}	25	$CuSO_4 \cdot 5H_2O$
Ni^{+2}	10	$NiCl_2 \cdot 6H_2O$
Fe^{+2}	20	$FeSO_4 \cdot 7H_2O$
$CaCO_2$	80	$CaCO_3$
$Mg^{+2}{}_2$	40	$MgCl_2$
Na_2CO_3	0	Na_2CO_3
Na_2SO_4	100	Na_2SO_4

[1] All sludge concentrations (volumes) are on dry weight basis and comparisons between methods were on a mg/l basis.

TABLE 3

COMPOSITION OF CONTRIVED WASTEWATER #2 (WW#2)

For Task III Screening Tests

Constituent	Concentration, mg/l	Chemical Used
Cr^{+6}	15	CrO_3
Cr^{+3}	30	$Cr(NO_3)_3 \cdot 9H_2O$
Cd^{+2}	1	$Cd(NO_3)_2 \cdot 4H_2O$
Cu^{+2}	25	$CuSO_4 \cdot 5H_2O$
Ni^{+2}	10	$NiCl_2 \cdot 6H_2O$
Fe^{+2}	20	$FeSO_4 \cdot 7H_2O$
$CaCO_2$	240	$CaCO_3$
Mg^{+2}	120	$MgCl_2$
Na_2CO_3	0	Na_2CO_3
Na_2SO_4	100	Na_2SO_4

TABLE 4

COMPOSITION OF CONTRIVED WASTEWATER #3 (WW#3)

For Task III Screening Tests

Constituent	Concentration, mg/l	Chemical Used
Cr^{+6}	15	CrO_3
Cr^{+3}	30	$Cr(NO_3)_3 \cdot 9H_2O$
Cd^{+2}	1	$Cd(NO_3)_2 \cdot 4H_2O$
Cu^{+2}	25	$CuSO_4 \cdot 5H_2O$
Ni^{+2}	10	$NiCl_2 \cdot 6H_2O$
Fe^{+2}	20	$FeSO_4 \cdot 7H_2O$
$CaCO_2$	0	$CaCO_3$
Mg^{+2}	0	$MgCl_2$
Na_2CO_3	381	Na_2CO_3
Na_2SO_4	100	Na_2SO_4

TABLE 5

COMPOSITION OF CONTRIVED WASTEWATER FOR TASK III COMPREHENSIVE STUDIES AND TASK IV

Constituent	Concentration, mg/l	Chemical Used
Cr^{+6}	56.8	CrO_3
Cr^{+3}	18.8	$Cr(NO_3)_3 \cdot 9H_2O$
Cd^{+2}	1.3	$Cd(NO_3)_2 \cdot 4H_2O$
Cu^{+2}	1.7	$CuSO_4 \cdot 5H_2O$
Ni^{+2}	1.0	$NiCl_2 \cdot 6H_2O$
Fe^{+2}	20.0	$FeSO_4 \cdot 7H_2O$
CN	10.0	KCN
$CaCO_3$	80	$CaCO_3$
Mg^{+2}	40	$MgCl_2$
Na_2CO_3	0	Na_2CO_3
Na_2SO_4	100	Na_2SO_4

Treatment of the wastewater using caustic in place of lime demonstrated the potential for reducing the sludge volume by as much as 60 to 75 percent; however, the sludge was characterized as having poor settling and handling characteristics.

While neither water softening nor segregated treatment of hexavalent chromium were found to have an appreciable effect on solids generation, chromium reduction using ferrous sulfate had greatly increased production of sludge. The results, presented in Table 6, show that the use of ferrous sulfate instead of sodium bisulfite resulted in 31 times more sludge. Further, the reduction reaction proceeded more slowly with ferrous sulfate as evidenced by the slow change in oxidation-reduction potential (ORP) during the treatment process. This slow reaction is likely to lead to the overaddition of ferrous sulfate, which would increase sludge generation even further.

Oxide precipitation and simultaneous cyanide oxidation using hydrogen peroxide demonstrated the potential for significantly reducing the dry weight of sludge produced during treatment. The sludge volume was comparable to that achieved by caustic treatment and the sludge exhibited superior settling and handling characteristics. Cyanide was found to be effectively destroyed simultaneously with precipitation, thus reducing the number of separate process steps required.

TABLE 6

EFFECT OF FERROUS SULFATE ON GENERATION OF SOLIDS[a]

Wastewater #	Treatment	pH	Settleable Solids, ml/l	Total Suspended Solids, mg/l
1	Combined $NaHSO_3$	2.5	37	1370
1	Combined $NaHSO_3$	2.5	39	--
1	Combined $NaHSO_3$	2.5	--	1145
1	Combined $NaHSO_3$	2.5	--	1215
1	Combined $FeSO_4$	3.3	160	29800
1	Combined $FeSO_4$	3.3	133	25400
1	Segregated $NaHSO_3$	2.5	35	1210
1	Segregated $NaHSO_3$	2.5	33	1190
1	Segregated $FeSO_4$	3.3	290	38000
1	Segregated $FeSO_4$	3.3	250	29000
2	Combined $NaHSO_3$	2.5	17	845
2	Combined $NaHSO_3$	2.5	17	832
2	Combined $FeSO_4$	3.3	135	42200
2	Combined $FeSO_4$	3.3	152	43000

[a]Combined treatment indicates that the entire wastewater solution containing all the metals was mixed prior to treatment for chromium reduction. Segregated treatment indicates treatment for chromium reduction of the wastewater containing only chromium prior to mixing with the other wastewaters. In both cases, the mixed wastewaters were treated with lime to precipitate metal hydroxides following chromium reduction.

Sodium borohydride treatment of the mixed metal wastewater also reduced the sludge volume to the level achieved by caustic treatment and oxide precipitation. In addition to chromium reduction, SBH treatment simultaneously reduces other metal ions to base metal.

The technologies tested in the screening study were then evaluated using the worth assessment model comparing 16 different characteristics of each process to the lime treatment baseline.

The two highest ranking technologies (sodium borohydride treatment and oxide precipitation) were selected for further testing. This second round of tests was more comprehensive and designed to provide statistically significant data to quantify their characteristics in terms of sludge produced.

In the second phase of testing, ozone was used as the oxidizing agent for oxide precipitation. The tests revealed, however, that ozone was so powerful an agent it caused trivalent chromium to reoxidize to the hexavalent state. Therefore, hydrogen peroxide was used for the remainder of oxide precipitation tests.

The quality of the effluent produced by oxide precipitation was very good. The sludge produced by oxide precipitation fell within 295.9 to 345.4 mg/liter of wastewater treated (95 percent confidence limits) with an average of 321 mg/liter. The weight difference of this sludge, as compared with that from lime treatment (985 mg/l) was determined to be significant with nearly 100 percent statistical confidence. However, the oxide sludge leached hazardous amounts of cadmium and chromium when subjected to the EP test and the sludge was unstable. After a sample of the wastewater containing sludge was allowed to stand overnight, it exhibited the yellow color characteristic of hexavalent chromium. Thus, even though hydrogen peroxide is a weaker oxidizer than ozone, it also is too strong an oxidizing reagent. This factor rendered simultaneous oxidation/precipitation unsuitable for practical application.

Analysis of the filtered SBH effluent showed that the process was capable of consistently producing effluent with metal concentrations below detection limits. The effluent, when decanted following clarification rather than filtered, was still of very good quality. Effluent data for the SBH treatment tests are presented in Table 7. These concentrations compare favorably to the EPA's effluent limits presented in Table 8.

The sludge produced by the SBH process fell within 293.7 to 323.6 mg/liter of wastewater treated (95 percent confidence limits), with an average of 309 mg/liter.

Again, the weight difference of this sludge, as compared with that from lime treatment (985 mg/l) determined to be significant with nearly 100 percent statistical confidence. However, as shown in Table 9, the sludge produced by SBH treatment leached hazardous amounts of both cadmium and chromium.

TABLE 7

EFFLUENT DATA FROM SODIUM BOROHYDRIDE TREATMENT TESTS

Sodium Borohydride Treatment Wastewater[a]

Run	TSS mg/l	TDS mg/l	Metals (mg/l)					
			Cr^{+6}	Cr Total	Cd	Cu	Ni	CN
1	314	2930	<0.05	<0.05	<0.01	<0.01	<0.1	<0.05
2	310	2370	<0.05	<0.05	<0.01	<0.01	<0.1	<0.05
3	286	2930	<0.05	<0.05	<0.01	<0.01	<0.1	<0.05
4	330	2380	<0.05	<0.05	<0.01	<0.01	<0.1	<0.05
5	306	2220	<0.05	<0.05	<0.01	<0.01	<0.1	<0.05
6	306	2670	<0.05	<0.05	<0.01	<0.01	<0.1	<0.05
7	-	-	-	0.44	0.01	0.02	0.1	-

[a]Runs 1-6 were treated with sodium borohydride and filtered using industrial filter media. Run 7 was unfiltered.

TABLE 8

U.S ENVIRONMENTAL PROTECTION AGENCY POINT SOURCE EFFLUENT LIMITATIONS[a]

Constituent	Daily Maximum, mg/l	Maximum 30 Day Average, mg/l
Chromium (total)	2.87	0.80
Cadmium (total)	1.29	0.27
Copper (total)	3.72	1.09
Lead (total)	0.67	0.23
Nickel (total)	3.51	1.26
Silver (total)	0.44	0.13
Zinc (total)	2.64	0.80
Cyanide (total)	1.30	0.28
Total Toxic Organics	0.58	--

[a]U.S. Environmental Protection Agency, Federal Register, V. 77, No. 169:38477, August 31, 1982.

TABLE 9

ANALYSIS OF SLUDGE PRODUCED BY SODIUM BOROHYDRIDE TREATMENT

Moisture Content and Leachability Study

Run[a]	Moisture (weight %)	EP Toxicity (mg/l) Cr	Cd	Cu	Ni
1,2	85.3	28.3	12.5	0.74	13.2
3,4	85.4	16.7	12.5	1.20	14.5
5,6	85.8	10.3	9.84	1.21	9.46

[a]Sludges from two runs were analyzed together to provide a sufficient amount of sludge for proper analysis.

Hydrogen gas is evolved during treatment with SBH and it is likely to be a function of the pH of the wastewater. Even though it could be eliminated with optimization of the treatment process, it nevertheless should remain a design consideration.

The oxide precipitation and SBH treatment technologies were again evaluated using these latest test results by another worth assessment model. Based on the stipulated criteria, SBH treatment was selected as the preferred technology. Although the cost of SBH is very high (currently in the range of $14.60/lb.to $17.00/lb. on a 100 percent basis for a stabilized water solution of 12 percent SBH), the reduced quantity of sludge (68 percent less) reduces hauling and disposal costs. A study of treatment system costs indicated that the economics of using SBH treatment are highly site-specific. Factors such as the type and efficiency of dewatering equipment and transportation and disposal costs must be considered. Detailed cost comparisons of SBH treatment and existing systems at the Air Force IWTPs indicate SBH treatment could not be economically applied at all five AF major maintenance centers. However, if the quantity of SBH required can be reduced by optimization studies, or if sludge transportation and disposal costs continue to increase or if present disposal sites close, the economics of SBH application could change. Thus, it is evident that to properly evaluate the SBH treatment technology, a site-specific assessment of current treatment system economics must be accomplished continuously as treatment system costs escalate.

Experimental Study of Methods For Rendering Sludge Nonhazardous

Many liabilities, as well as costs, are associated with the generation and disposal of hazardous sludge. Thus, the

advantage not only lies in minimizing the volume of hazardous sludge, but also in treating the sludges produced to render it nonhazardous. This is the aim of Task 4.

Since SBH treatment may or may not be economical at any given site, the following three sludge types are being tested under this task (still in progress): lime treatment, caustic treatment, and SBH treatment. Thus, the results of this task may be applied to sites using any of these three treatment processes whether or not SBH would be economical. The application of results from this task may, however, affect the economics of employing SBH treatment because delisting a sludge would reduce the total treatment costs.

Potential processes were selected for screening tests based upon information gathered from literature. Five processes were tested initially and these are described briefly below:

1. Solidification: The sludge produced is solidified by combination with a mixture of Portland cement and fly ash.

2. Heat treatment: The sludge is treated by heating and drying under controlled conditions of time and temperature.

3. Leaching: The sludge is treated to selectively leach components for recovery.

4. Barium compound addition: The wastewater is treated with barium-based compounds to stabilize the sludge based on similar process applications identified in existing patents.

5. Sludge aging: The sludge is allowed to age exposed to a sheltered environment.

Data and observations from the screening tests were used in another worth assessment model and three technologies were selected for further testing. Further, a fourth technology was identified at this time and added to the list as follows:

- Barium compound addition
- Heat treatment
- Solidification
- Sludge washing

While barium compound addition did not fare well in the initial screening tests, it was selected due to its simplicity of application. Optimization studies showed the addition of barium acetate could reduce the level of chromium that leached, but the sludge still remained hazardous. Use of barium carbonate increased the leachability of the sludge.

Heat treatment was investigated as a method of reducing both the volume and toxicity of the sludge. The volume reduction that occurs is primarily a result of water loss, whereas a reduction in toxicity would be a result of physical and/or chemical changes in the sludge. These physical/chemical changes, considered to be mainly a collapse of the gelatenous structure of the sludge, were observed during sludge drying in a previous project (AES/EPA Cooperative Agreement). It was hypothesized that this process could be accelerated by the application of heat.

Results of the heat treatment studies indicate that temperature has a significant effect on the leaching of metals, particularly chromium and nickel. Over a specific time, if temperature is increased, the metals leaching from the sludge decrease to very the leachability increased, as shown graphically in Figure 1. While complete sample drying at 120°C took approximately 2 hours, the leaching was minimized after one hour of treatment.

The results of these tests show that heat treatment may be a viable means of rendering sludge nonhazardous, but this depends on the sludge composition. A high degree of process control would be required to ensure that the treated sludge would be nonhazardous. Although this technology would require some energy input, it could be provided by a low level waste heat source. In addition to "detoxification," the sludge volume decrease would further reduce transportation and disposal costs.

To date, solidification has made two types of sludges nonhazardous: lime and SBH. Solidification tests using caustic sludge are currently underway.

In evaluating the solidification experiments, the solidified samples were first subjected to the EPA integrity test. This impact test breaks the solidified sludge and then the pieces are run through the EP test.

Tests to date have indicated that up to 18.2 percent SBH sludge and 47.7 percent lime sludge can be mixed with Portland cement and fly ash and be rendered nonhazardous. The higher sludge percentage for lime mixtures can be attributed to the good bonding characteristics of the lime sludge, cement, and fly ash.

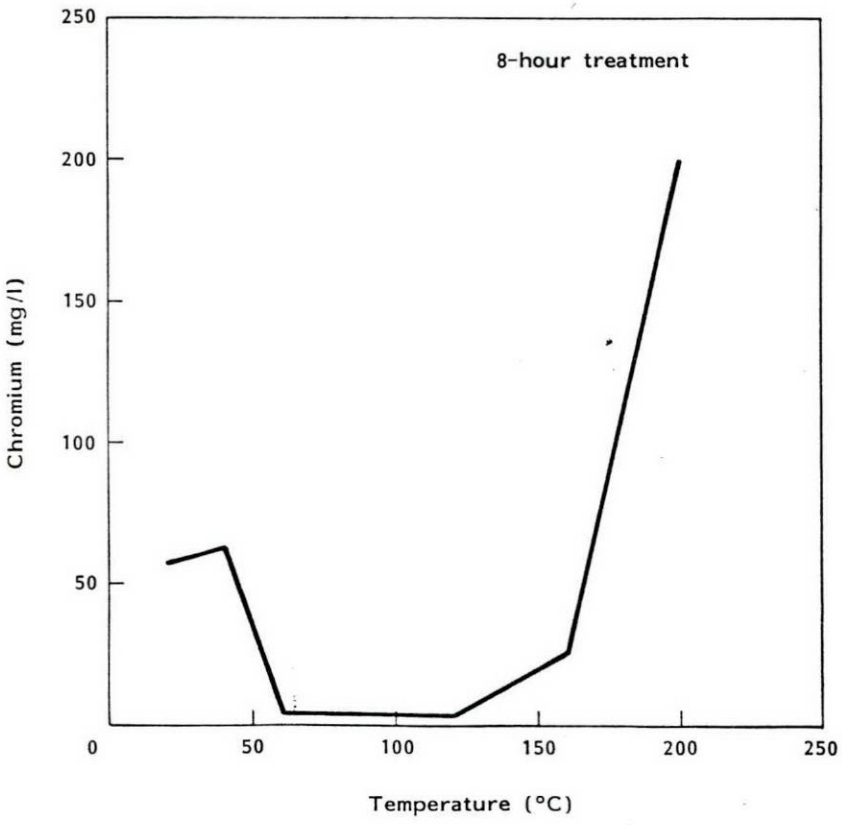

Figure 1. Heat Treatment Temperature Study - EP Results for Chromium

As with SBH, the economics of employing solidification are highly site specific. A detailed economic evaluation of transportation and disposal costs and a subjective evaluation of liability would be required to assess the applicability of this technology. Liability would be particularly important if the sludge were disposed of in a landfill owned or operated by the plater.

Sludge washing is also being tested. Initially, it was hypothesized that washing the sludge with a dilute ammonium chloride solution would cause collapse of the gelatinous structure of the sludge and reduce its leachability. Tests to date, however, have indicated that although the leachability of the sludge is not reduced, its dewaterability is enhanced by the washing

process and the wash solution does not require treatment following the process. Additional tests using water for washing are currently being performed. Preliminary results indicate that this procedure may also be effective in improving the dewaterability of the sludge. This is particularly significant in that the volume of sludge for disposal could easily and inexpensively be reduced if the procedure proves to be effective in repeated tests.

Conclusions and Summary of Results

The results from this project indicate that innovative technologies may be economically applied to both reduce the volume of mixed metal electroplating treatment sludges and render these resulting sludges nonhazardous. However, the economics associated with employing these technologies are highly dependent on site-specific factors and warrant a detailed study of total treatment costs before application. Further, with increasing treatment and/or disposal costs, reevaluation of these technologies is warranted. The more important results obtained from studies performed to date under this project are as follows:

1. The use of ferrous sulfate, rather than sodium bisulfite, for the reduction of hexavalent chromium results in a dramatic increase in sludge generation. The increase from ferrous sulfate was 31 times the amount of sludge produced by the bisulfite process.

2. The use of caustic in place of lime for the precipitation of metals as hydroxides results in a reduced quantity of sludge. The sludge, however, without additional treatment, does not settle as well as the lime sludge and is perceived to be more difficult to handle because of the delicate nature of the floc.

3. Oxide precipitation and simultaneous cyanide oxidation using hydrogen peroxide or ozone should produce an effluent of good quality when applied to non-chromium mixed metal wastewaters; however, if chromium is present, it will reoxidize to the hexavalent state.

4. Sodium borohydride treatment of mixed metal wastewaters is capable of producing a high quality effluent without filtration, or an effluent with metal concentrations below detection limits when filtered with industrial filter media.

5. Substitution of SBH treatment for lime treatment of mixed metal wastewaters can result in a 68 percent sludge reduction. This is illustrated graphically in Figure 2. The economics of employing the SBH treatment technology are highly dependent on site specific factors. Economic applicability of the technology must therefore be evaluated on a case-by-case basis.

6. Heat treatment was determined to be a viable process for rendering SBH sludge nonhazardous if subjected to strict control.

7. Solidification was determined to be effective in rendering both lime treatment and SBH sludges nonhazardous. The maximum aggregate substitution for each sludge on a dry weight basis, was determined to be 47.7 percent lime sludge and 18.2 percent SBH sludge.

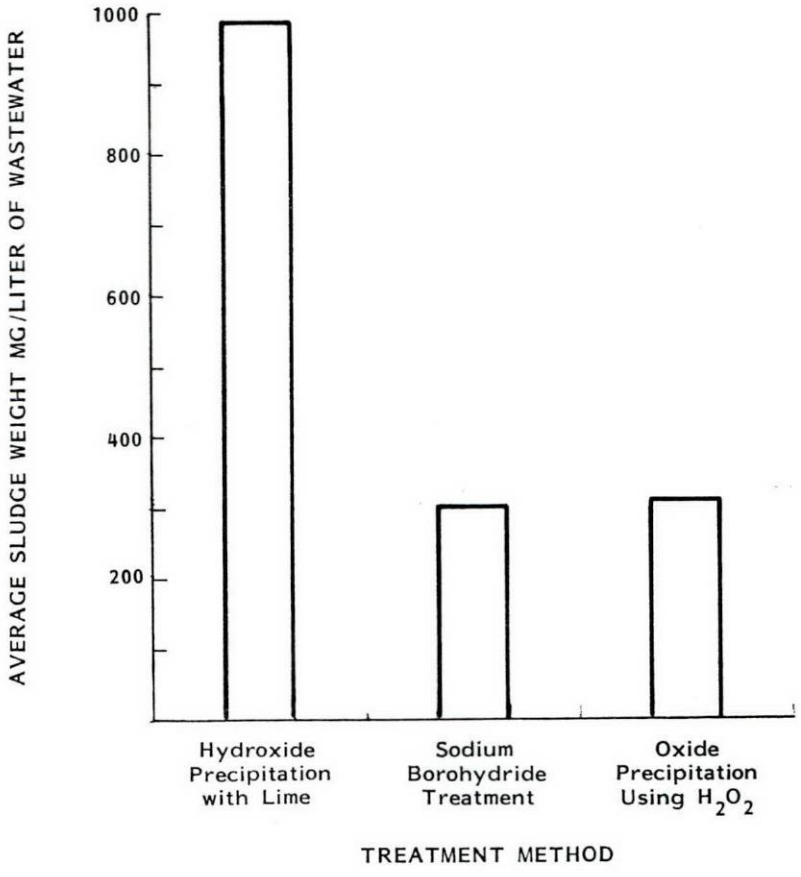

Figure 2. Comparison of Dry Weights of Sludge Produced by Treatment Methods Tested, Average Sludge Weight mg/liter of Wastewater Treated vs. Treatment Method.

A-5

Research Session A

Influence of Magnetic Fields on the Electrodeposition of Chromium

Dr. John Dash, Ru-Tsin Chen and K Housen
Portland State University
Portland, OR

INFLUENCE OF MAGNETIC FIELDS ON THE ELECTRODEPOSITION OF CHROMIUM

J. Dash, Ru-Tsin L. Chen and K. Housen
Physics Department, Portland State University
Box 751, Portland, Oregon 97207

Abstract

It is shown that magnetic fields increase the current efficiency of chromium deposition, and reduce the volume of hydrogen gas produced. These effects are attributed to the Lorentz force on ions which causes visible convection in the electrolyte. This convection apparently lowers the cathode temperature sufficiently to account for the observed increase in chromium deposited and reduction in hydrogen evolved.

Introduction

In recent years, a number of investigators have reported that magnetic fields applied during electrolysis produce very significant effects on various aqueous electrolytic processes. Laforgue-Kantzer concluded that a Hall effect occurs in aqueous electrolytes (1). This effect was attributed to the Lorentz force on protons which were postulated to have a finite life-time in the un-hydrated state. The basis for the explanation of her results was that the un-hydrated proton has a velocity which is about 10^5 times as large as the drift velocity. In her model, the drift velocity of the proton is represented as a composite of the relatively slow velocity in the hydrated state and the extremely high velocity in the un-hydrated state. Virlan and Parsadanjan reported that iron deposited electrolytically in the presence of a magnetic field has very significantly increased hardness and reduced porosity (2). They attributed these effects to magnetohydrodynamic sweeping of H_2 molecules off of the deposit.

A report by Perakh shows that nickel and iron-nickel films deposited in a magnetic field have greatly different macrostresses compared with films deposited without a magnetic field (3). This report hypothesizes that changes in the macrostress level may be caused by changes in the amount of hydrogen gas produced during electrodeposition, although the author stated that it was unclear why a magnetic field changes the amount of hydrogen co-deposited with the metal. The results of references (2) and (3) are consistent with Laforgue-Kantzer's work, i.e., they can be understood if protons are preferentially deflected away from the cathode by a magnetic field.

Dash et.al. showed that magnetic fields improve the uniformity of electrolytic thinning in the preparation of specimens for electron microscopy (4). In a later report Dash and King reported that magnetic fields improve the uniformity of copper deposits and simultaneously reduce the resistance of the copper deposition cell (5). These authors also determined the effect of magnetic field orientation on the profiles produced by anodic thinning and by cathodic deposition. Gak and Rokhinson found that a magnetic field of 4 kG doubles the limiting current for deposition from 0.1 N $CuSO_4$, 0.1 N $CuCl_2$, and 0.1 N $NiSO_4$ (6). They also determined that the current density above which powder-type deposition occurs increases continuously with magnetic field strength in the range zero to 12 kG. As an example, a field of 4 kG allows deposition of compact copper at 40 percent higher current density than

zero applied field. In studies of flow cells, Mohanta and Fahidy found that the imposition of a uniform magnetic field can prevent the existence of limiting currents at moderate Reynolds numbers (7).

As originally observed by Frary (8), magnetic fields cause circulation of electrolytes during electrolysis due to the force on moving charged particles. The electrolyte circulates around the magnetic flux lines, as expected from the Lorentz force (equation 1 below). This circulation is analogous to mechanical stirring, and it therefore should reduce the concentration overpotential and increase the limiting current. An important difference compared with mechanical stirring is that magnetic stirring persists through the double layer until the moment when ionic discharge occurs or it begins at the moment when an ion is formed on the surface of an electrode. In comparison, mechanical stirring is not effective within the adsorbed layers of liquid on the electrodes. Thus, it should be expected that, if the magnetic force is significant compared with the electrical force on ions, then there must be significant effects on electrode processes (including adsorption and surface diffusion) in the presence of an applied magnetic field.

In the presence of electric and magnetic fields, the Lorentz force on an individual ion in the electrolyte is given by (1):

$$\vec{F} = q\,(\vec{E} + \vec{v} \times \vec{B}) \qquad (1),$$

where $\vec{F}$ = Lorentz force on an ion,

q = ion charge,

$\vec{E}$ = electric field,

$\vec{v}$ = ion velocity, and

$\vec{B}$ = magnetic field.

If only an electric field is present, an ion moves in the direction of the electric field. When a magnetic field is superimposed, the magnetic component of the Lorentz force causes the ion to circulate around the direction of the magnetic field. Positive ions and negative ions move in opposite directions in the electric field. Because their motion and their charges are opposite, the magnetic force on them is in the same direction. This produces circulation of the electrolyte (8).

An estimate of the magnitude of the magnetic force acting on the bulk electrolyte to produce circulation can be made as follows. In an electrolyte the total moving charge per unit volume is given by

$$\frac{q}{v} = \frac{i_1}{v_1} + \frac{i_2}{v_2} + \ldots + \frac{i_n}{v_n} \qquad (2),$$

where q is the charge (C), V is the volume (cm^3), i_1, i_2, . . . i_n are the individual ionic current densities at an electrode (A/cm^2), and v_1, v_2, . . . v_n are the magnitudes of the individual ionic velocities (cm/sec).

Assuming B normal to v_1, v_2, . . . v_n, the magnitude of force per unit volume of electrolyte is

$$\frac{F}{V} = \left(\frac{i_1 v_1}{v_1} + \frac{i_2 v_2}{v_2} + \ldots \frac{i_n v_n}{v_n}\right) B$$

$$= (i_1 + i_2 + \ldots + i_n)\, B$$

$$= iB \qquad (3),$$

where B is the magnitude of the magnetic field and i is the total current density at the electrode.

For $i = 10^{-1}$ A/cm^2 and $B = 10^4$ gauss, $\frac{F}{V} = 100$ dynes/cm^3.

This force is opposed by frictional forces, so the rate of bulk circulation depends on the viscosity of the electrolyte.

Even in the absence of bulk circulation of the electrolyte, magnetic fields produce significant effects on electroysis (9,10). For example, in five similar experiments with applied magnetic field of 3.3 kG, a total of 30 Leclanché cells in the magnetic field produced 24 per cent more energy than 30 similar cells discharged under the same conditions with no applied magnetic field. The power for the cells in the magnetic field was continuously greater for the first 100 minutes of discharge in all five of these experiments (10). Here, circulation is absent, due to the high viscosity of the electrolyte. According to accepted theory (11), the rate-limiting reaction depends on proton motion to the cathode and the subsequent polarization produced by the reaction products. If proton motion to the cathode is inhibited by magnetic fields, then some other (as yet undetermined) reaction must become rate-limiting.

The results in references (1,2,3,9,10) are all consistent with the hypothesis that magnetic fields preferentially inhibit proton motion to the cathode in a wide variety of electrolytic cells. In the present work, another system was chosen in which hydrogen co-deposits with a metal, namely, electro deposition of chromium from aqueous CrO_3 solutions. Measurements were made of the quantity of chromium deposited and of hydrogen gas produced as a function of the applied magnetic field strength.

Experimental

Figure 1 shows a diagram of the circuit used for electrolysis. All experiments were performed at constant current, with the cell in the magnetic field connected in series to the cell outside the field. Thus, the current through both cells was exactly the same in each experiment. The potential difference across each cell was recorded continuously for all experiments. The cell used for current efficiency experiments is illustrated in Figure 2, and Figure 3 shows the cell used to measure hydrogen evolution. Table 1 gives other experimental conditions for both types of experiments.

Magnetic fields greater than one kG were applied with an electromagnet (Varian Model V4004), and fields below one kG were applied with either a Variflux permanent magnet (Laboratory for Science Model 2) or with the electromagnet. The magnitude of the magnetic field was determined for each experiment with a Bell Model 620 gaussmeter (accuracy $\pm$ 1.5 percent). The variation of the field within the gap is included in Table 4.

Some temperature data were taken with a thermometer and some were taken with a thermocouple, both of which were calibrated.

The standard chromic acid electrolyte, containing 250 gm CrO_3 per liter and a ratio of CrO_3 to sulphate ion of 100:1, was used in all experiments. The electrolyte was changed after each nine-hour deposition experiment and after four hydrogen evolution experiments.

The cathodes were all cut from 25 μm-thick nickel (0.9999 Ni). These

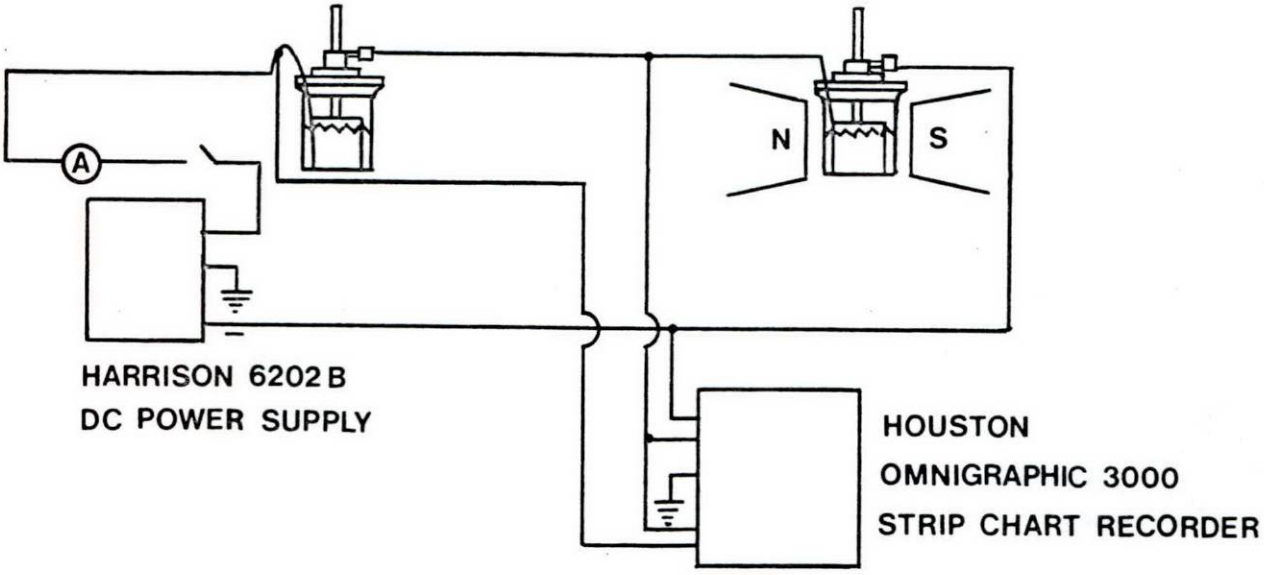

Figure 1
Diagram of the circuit used for both the current efficiency and the hydrogen evolution experiments.

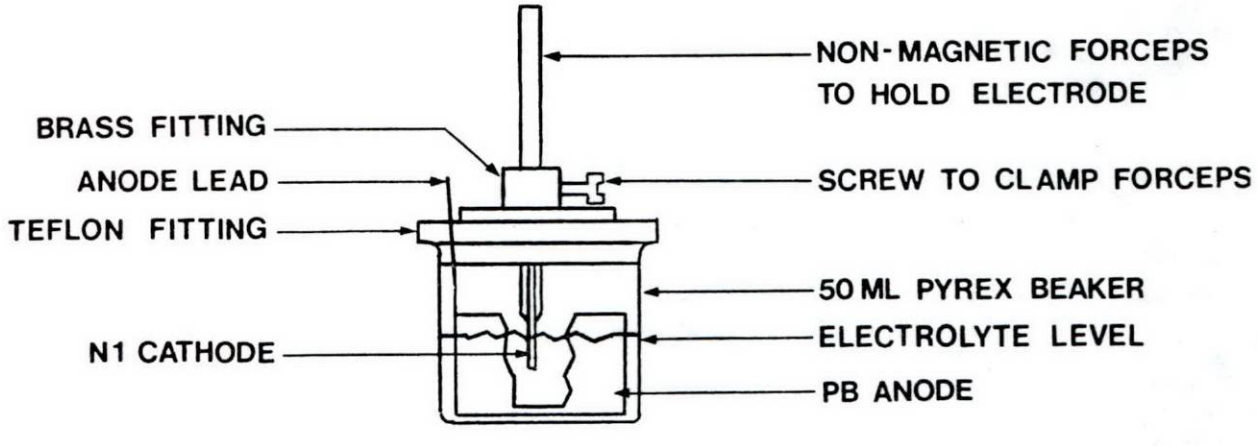

Figure 2
Diagram of the cell used for experiments on the current efficiency of chromium deposition.

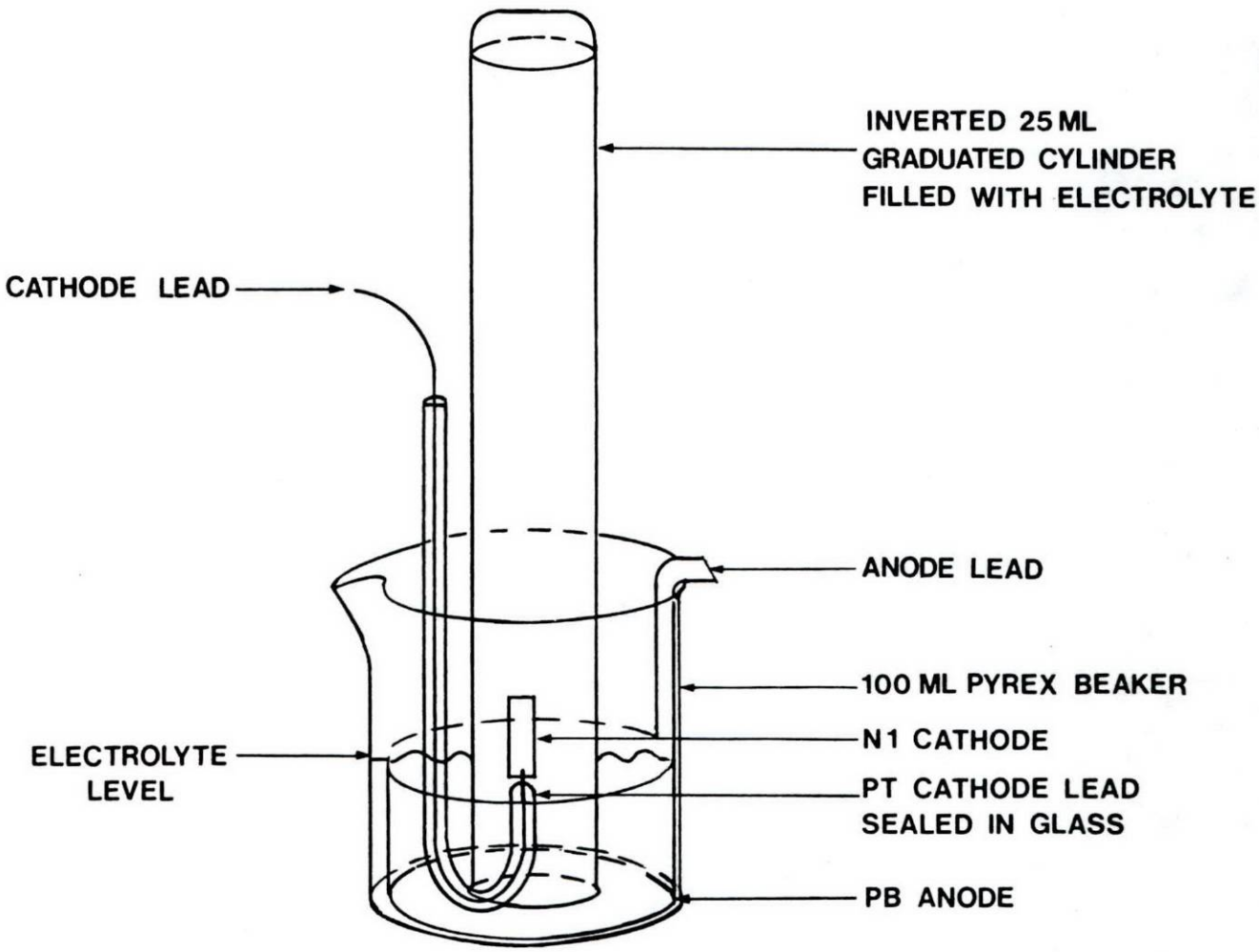

Figure 3
Diagram of the cell used for experiments on hydrogen evolution during chromium deposition. The nickel cathode is spotwelded to the platinum lead wire.

EXPERIMENTAL CONDITIONS	TYPE OF EXPERIMENT	
	Current Efficiency	Hydrogen Evolution
Current (ma, $\pm$ 0.5)	180	270
Surface Area of Cathode Immersed in Electrolyte (cm^2 $\pm$ 0.05)	0.3	0.45
Approximate Current Density at Cathode (amp/cm^2)	0.3	0.3
Time	9 hours $\pm$ 0.01	25 minutes $\pm$ 0.1
Size of Lead Anode	Diameter 3.3 cm Height 3.8 cm	Diameter 3.7 cm Height 2.15 cm

Table 1

Conditions used for current efficiency and hydrogen evolution experiments.

were cleaned ultrasonically with a detergent, rinsed with distilled water, and air-dried. The cylindrical lead anode (0.99999 Pb) was chemically polished after each experiment by immersing in a solution of 20 percent H_2O_2 (30 percent) and 80 percent glacial acetic acid for ten seconds, rinsing in distilled water, and air-drying. New cathodes were used for each experiment.

Hardness tests were made on cross sections of cathodes from the current efficiency experiments with a Tukon hardness tester using a Knoop indenter under a load of one kG. The electrodes were first mounted in epoxy and heated for 69 hours at 96 C in an effort to reduce the amount of hydrogen present in the deposits and possibly develop porosity. After this heat treatment, the mount was ground and polished to produce a smooth, plane surface.

Results

1. Current efficiency experiments. The results for six experiments are given in Table 2. Because the current efficiency for chromium deposition decreases rapidly with increasing electrolyte temperature (12), it is essential to refer data for deposition in and outside a magnetic field to the same electrolyte temperature. In all experiments, the electrolyte temperature at the start was closely the same for the cell in the field and the cell outside the field. For experiments one and two, in which the permanent magnet was used, the final electrolyte temperature for the cell in the field was about 0.8 C lower than for the cell outside the field, due in part to the magnet polepieces. In experiments three to five, this effect is more pronounced because the field was applied with a water-cooled electromagnetic and the polepieces were below room temperature. In experiment six, the effect of the polepieces is less because the higher magnet current required for the eight kG field warmed the cooling water to room temperature or higher.

A plot of the current effeciency versus temperature data for B = 0 is given in Figure 4. Using the line in this plot, which was determined by the method of least squares, the data for each experiment were corrected, and the averaged results are given in Table 3. This shows that magnetic fields in the range 0.8 to eight kG significantly increase the current efficiency for chromium deposition.

Except for the first two minutes, the cell potentials decreased linearly with time. The total decrease in each experiment was about 0.05 v. The average potential given in Table 2 ignores the spike (about 0.3 v high) which was present at the beginning of every experiment for both cells. The lack of dependence of cell potential on the magnitude of the applied magnetic field in these results is in contrast to the case of copper deposition at similar current densities, where concentration overpotential is large (5). This suggests that concentration overpotential is absent in chromium deposition due to convection induced by the formation and dispersion of gas at the electrodes, as noted previously in the case of nickel electrowinning (13).

The main difference in appearance of the deposits made in a magnetic field compared with those produced without a field is that the former have more uniform color from top to bottom of the deposits. All deposits (except that made with B = 8 kG, experiment 6) have a light gray color at the top of the electrode and a dark gray color at the bottom. The extent of the light gray zone decreases with increasing magnetic field strength until it disappears at 8 kG (Figure 5). This effect is caused by motion of the electrolyte induced by the Lorentz force on ions, as described above.

The results of hardness tests on the electrodes shown in Figure 5 are

EXPT.	FIELD (kG)	AVERAGE CELL POTENTIAL (v ± 0.005)	MASS OF CHROMIUM DEPOSIT (gm ± 0.0001)	ELECTROLYTE TEMP. (C ± 0.1) Initial	Mean	Final	CURRENT EFFICIENCY (gm/coulomb ± 0.002 X 10^{-5})
1	0	3.07	0.1931	21.4	22.7	23.9	3.31 X 10^{-5}
	0.763	3.07	0.1957	21.5	22.3	23.1	3.36
2	0	3.07	0.1894	22.8	24.3	25.9	3.25
	0.763	3.07	0.1921	22.6	23.8	25.0	3.29
3	0	3.06	0.1779	23.5	25.2	27.0	3.04
	2	3.05	0.1912	23.5	24.1	24.7	3.27
4	0	3.01	0.1694	23.0	25.3	27.5	2.91
	2	3.05	0.1914	23.0	23.5	24.0	3.28
5	0	3.02	0.1741	25.5	26.3	27.0	2.99
	2	3.08	0.1928	25.0	25.0	25.0	3.30
6	0	3.03	0.1787	25.4	25.7	26.0	3.06
	*8.0	3.07	0.1944	24.7	25.1	25.5	3.33

Table 2

Effect of a magnetic field on the current efficiency of chromium deposition. The field was normal to the cathode surface in experiment 1 and parallel to the cathode surface in all other experiments.

* In this experiment the field in the magnet gap ranged from 8.00 to 8.45.

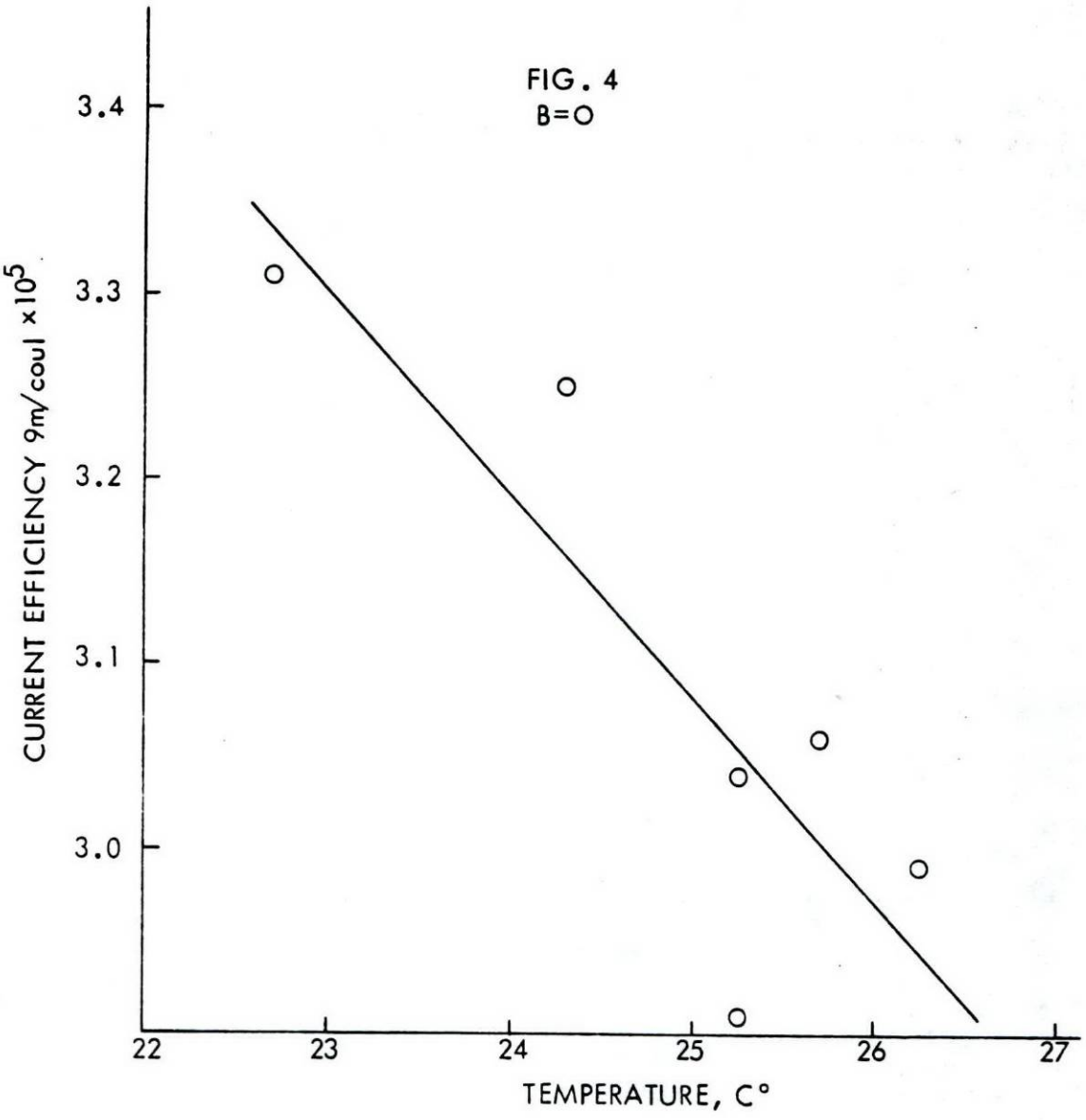

Figure 4

Current efficiency of chromium deposition versus temperature for the cell outside the magnetic field. The line in the figure was calculated by the method of least squares.

FIELD (kG)	NUMBER OF EXPERIMENTS	AVERAGE TEMP °C	CURRENT EFFICIENCY gm/coulomb		INCREASE DUE TO B %
			In Field	Outside Field	
0.763	2	23.1	3.33×10^{-5}	3.29×10^{-5}	1.2
2.0	3	24.2	3.28	3.17	3.5
8.0	1	25.1	3.33	3.07	8.5

Table 3

Effect of a magnetic field on current efficiency of chromium deposition. Figure 4 was used to obtain the data for current efficiency at B = 0.

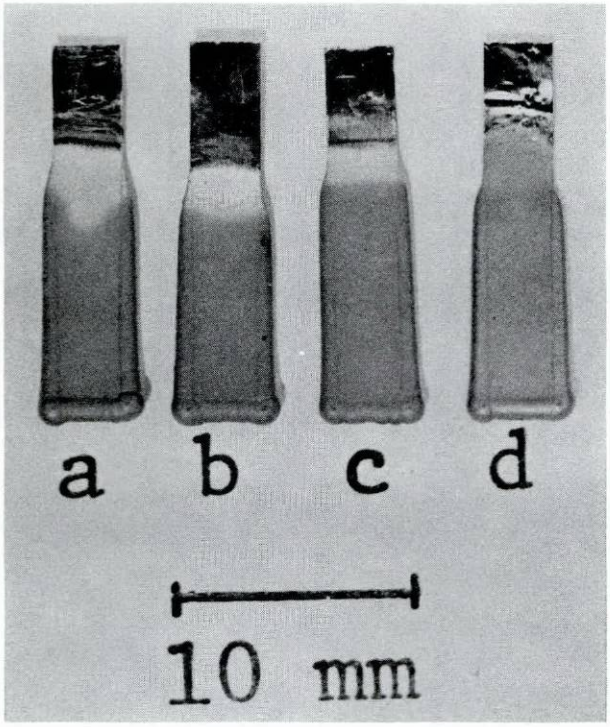

Figure 5

Effect of a magnetic field on the appearance of chromium deposits: (a) B = 0; (b) B = 0.8 kG; (c) B = 2 kG; (d) B = 8 kG.

given in Table 4. These data indicate that a magnetic field has only a small effect on the average hardness, but it significantly improves the uniformity of hardness. For example, hardness ranged from 633 to 670 KHN for electrode b (deposited in a field of 0.8 kG) compared with 621 to 706 KHN for electrode a (no magnetic field during deposition). These two deposits have the same average hardness. The lowest average hardness was obtained for electrode d, (deposited in a field of 8 kG), and the highest was for electrode c (deposited in a field of 2 kG). There was no obvious effect of a magnetic field on the amount or porosity in the polished cross sections.

2. Hydrogen evolution experiments. The data for these experiments is summarized in Table 5. This data represents 24 experiments, in each of which the hydrogen produced during chromium deposition was measured for one cell in a magnetic field and for a similar cell connected in series outside the field. The magnetic field was parallel to the cathode surface in all of these experiments. In only one of these experiments was a greater volume of hydrogen produced by the cell in the magnetic field. The data for the experiment in which this occurred is given below:

B kG, ± 0.005	H_2 Produced ml, ± 0.1	Temperature °C, ± 0.1 initial	final	Time min., ± 0.1	Source of Field
0	23.2	24.4	26.5	25	-
0.25	23.6	24.5	26.7	25	permanent magnet

For the cells outside the magnetic field the electrolyte temperatures ranged from 22.8°C (minimum initial temperature, T_i) to 28.2°C (maximum final temperature, T_f). The average temperature for all experiments outside the field $\left(\frac{\text{av. } T_i + \text{av. } T_f}{2}\right)$ was 25.3°C. The temperature range for all experiments in the field was 22.8 C to 27.6°C, and the average temperature was 24.7°C.

The volume of hydrogen produced by cells outside the field ranged from 23.2 ml to 24.4 ml, and the average for all experiments outside the field was 23.9 ml. For cells in the field, the range was 20.1 ml (at 7 kG) to 23.7 ml (at 0.25 kG), and the average for all experiments in the field was 22.4 ml. In these results there is no regular increase in volume of hydrogen produced with increasing temperature. For example, the group 3, no field experiments (Table 5) at an average temperature of 26.2°C produced less hydrogen than the group 4, no field experiments at an average temperature of 24.9°C. However, there is a definite decrease in volume of hydrogen produced with increasing magnetic field strength, as shown in Figure 6.

Discussion of Results

Our measurements show that a magnetic field slightly increases the current efficiency of chromium electrodeposition. The convection of the electrolyte caused by the magnetic field enhances heat dissipation from the electrodes (14). Thus, the electrodes in the cell located in the magnetic field tend to run approximately 1°C cooler than the electrodes in the cell outside the magnetic field. This should enhance chromium deposition efficiency, because of its strong temperature dependence, Fig. 4. For example, the data

Specimen	Trans. KHN		Long. KHN		Av. KHN (Long and Trans) / 2
	Av.	Range	Av.	Range	
a (B=0)	666	641-706	645	621-670	656
b (B=0.8kG)	662	649-670	649	633-666	656
c (B=2kG)	670	645-702	662	645-684	666
d (B=8kG)	658	645-688	645	633-684	652

Table 4

Hardness of electrodes shown in Fig. 5. Knoop hardness numbers (KHN) were determined with a Tukon hardness tester, using a one kG load. Twenty readings were taken in a cross section of each electrode approximately eight mm from the top. Ten were parallel and ten were perpendicular to the plane of the electrodes.

GROUP	B(kG)	H_2 PRODUCED (ml ± 0.1)			AVERAGE ELECTROLYTE TEMPERATURE (C ± 0.1)		
		Ave.	range Min.	Max.	Initial	Mean	Final
1	0	23.7	23.2	23.9	25.0	25.8	26.5
	0.25 ± 0.005	23.5	23.3	23.7	24.5	25.6	26.7
2+	0	23.8	23.4	24.2	24.9	25.7	26.5
	0.5 ± 0.02	23.3	23.0	23.5	24.8	25.7	26.5
3	0	23.9	23.9	24.2	25.6	26.2	26.8
	0.5 ± 0.02	23.0	22.8	23.4	25.3	25.5	25.6
4	0	24.1	23.8	24.2	23.8	24.9	26.0
	1.0 ± 0.03	22.9	22.4	23.1	23.7	24.3	24.8
5	0	23.7	23.3	24.0	22.4	23.6	24.7
	1.75 ± 0.05	21.9	21.8	22.0	22.2	22.8	23.3
6	0	24.2	23.9	24.4	25.3	26.1	26.8
	3.50 ± 0.08	21.0	20.4	21.6	24.5	25.2	25.8
7+	0	23.5	23.4	23.5	23.4	24.3	25.1
	7.0 ± 0.1	20.5	20.1	20.8	22.8	23.5	24.1

Table 5

Effect of a magnetic field on the volume of hydrogen co-deposited with chromium. Group 1 and 2 experiments were performed with the permanent magnet and all others were performed with the electromagnet. The averages are for four experiments, except for groups 2 and 7 (+) in which only two experiments were performed.

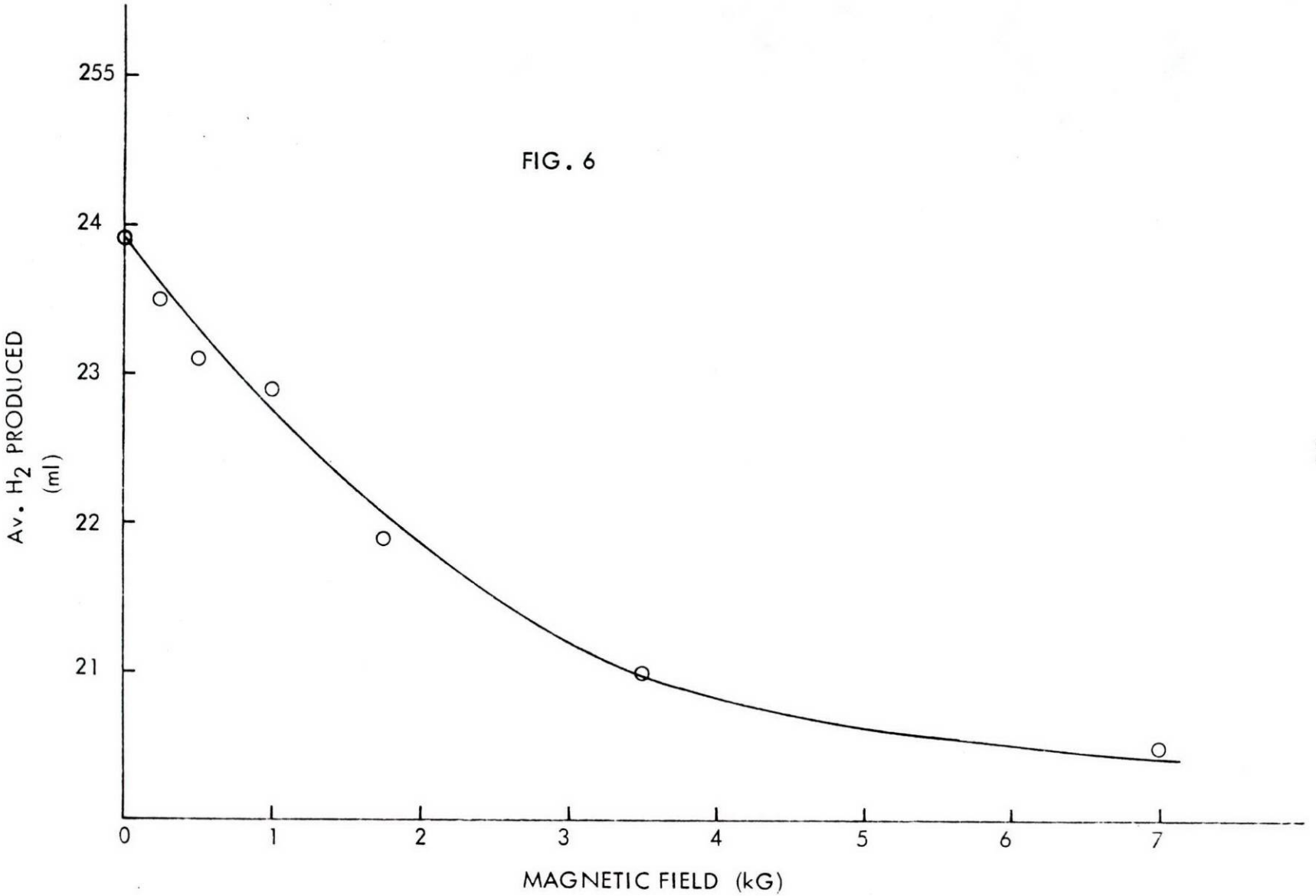

FIG. 6

Figure 6. Effect of a magnetic field on the volume of hydrogen produced during deposition of chromium.

in Table 3 at 2 kG show that the average current efficiency obtained for the cell in the magnetic field was 0.11 X 10^{-5} g/C greater than for the cell outside the magnetic field. From Fig. 4, it is apparent that this increase in current efficiency can be obtained by a decrease in electrolyte temperature of 1°C. We suggest that the effect of convection caused by the applied magnetic field is to lower the temperature of the cathode by approximately 1°C compared with the cathode temperature in the cell outside the magnetic field, even though the bulk electrolyte in both cells is at the same temperature.

Fig. 6 indicates that a magnetic field of 2 kG reduces the amount of hydrogen gas collected by about 2 ml (after passage of 405 coulombs). The magnetic field causes visible swirling of the gas bubbles in the electrolyte, resulting in dissolution of some of the gas and passage outside the collection tube of some of it. These latter two effects probably reduce the volume of hydrogen gas collected by about 0.2 ml (14). The current consumed by the enhanced deposition of chromium accounts for about one-third of the reduced hydrogen volume. It is possible that the remainder of the current resulting from reduced hydrogen formation may have been consumed in enhancing the formation of Cr (III) at the cathode, but we did not measure Cr (III).

A recent study concluded that a magnetic field promotes the discharge of molecular hydrogen during cathodic charging and inhibits the diffusion of atomic hydrogen into steel (15). These effects occur in the absence of competing cathode reactions. In our experiments, competing cathode reactions are favored by reduced temperature. Convection of the electrolyte induced by the magnetic field reduces cathode temperature, thus enhancing chromium deposition and inhibiting discharge of molecular hydrogen. We have no information on the hydrogen content of the deposits, but the long deposition time probably permitted saturation of all deposits with hydrogen.

Acknowledgements

We are grateful to J. Tung, D. DeSart, and D. Collins for their contributions to this study. This research was supported in part by the U.S. Army Research Office.

References

1. D. Laforgue-Kantzer, Electrochim. Acta, 10, 585 (1965).
2. A.I. Virlan and A.S. Parsadanjan, Energetics and Electronics, (Russian), Trudy 9, p. 3 (Kishinevo Polytechnical Institute, U.S.S.R, 1968).
3. M. Perakh, J. Electrochemical Soc., 122, 1260 (1975).
4. J. Dash, R.W. Roeter, and W.W. King, "Proceedings 27th Annual Meeting of Electron Microscopy Society of America," P. 144 (Claitor's Publishing Div., Baton Rouge, 1969).
5. J. Dash and W.W. King, J. Electrochemical Soc., 119, 51 (1972).
6. E.Z. Gak and E. Kh. Rokhinson, Elektronnaya Obrobat. Mat (Russian), 1, 68 (1974).
7. S. Mohanta and T.Z. Fahidy, Electrochim. Acta, 19, 835 (1974).
8. F.C. Frary, J. Am. Chem. Soc., 29, 1592 (1907).
9. W. Socha and J. Dash, Extended Abstracts of Electrochemical Soc., 75-2, 45 (1975).
10. W. Socha, M.S. Thesis, Portland State University, 1976.
11. D.B. Matthews, Rev. Pure and Appl. Chem., 20, 103 (1970).

12. W. Hume-Rothery and M.R.J. Wyllie, Proc. Royal Soc., 181a, 331 (1943).
13. O. Wassef and T.Z. Fahidy, Electrochim. Acta, 21, 727 (1976).
14. C.A. Cousins, M.S. Thesis, Portland State University, 1982.
15. V.S. Agarwala and J.J.DeLuccia, Report No. NADC-81029-60, Naval Air Development Center (1981).

A-6

Research Session A

Plating on Titanium: Process and Applications

Dr. Martin Thoma
MTU Motoren-und Turbinen Union
Munchen GmbH
Munchen, W. Germany

PLATING ON TITANIUM - PROCESS AND APPLICATION

Martin Thoma

MTU Motoren- und Turbinen-Union München GmbH

München, West Germany

INTRODUCTION

Electroplating on titanium and titanium alloys with good adhesion of the platings to the substrate has been made possible by special activation of the titanium alloys (1). The process is simple to be carried out and it is reproducible. Hence, this method can be used for the application of functional electroplatings to titanium and titanium alloys.

Applications required are the following ones:

Salvaging of components/Restoring of dimensions required

Protection against wear

Tribological coatings

Protection against stress corrosion cracking

Protection against oxidation at elevated temperatures.

PLATING PROCESS

Experimental procedure

The titanium alloys used for testing are Ti6Al4V, Ti2Cu, IMI 685, Ti6Al2Sn4Zr2Mo and pure titanium (Table 1).

The platings were deposited using common electroless and electroplating baths.

The plating process requires the following operation sequences: Vapour degreasing, Blasting, Pickling, Activating and Plating. The process parameters are shown in Table 2.

An advantage of the process is, in contrast to conventional processes, that plating must not be carried out immediately after activation. This type of activation guarantees a properly bonded deposit without the need for an intermediate layer. Pickling and activation processes are combined with stock loss. Pickling removes material at the rate of approximately 3 µm per area, and activation at approximately 3 µm per area, i. e. total stock loss of about 6 µm.

The different steps of the process result in special surface conditions clearly to be recognized by visual inspection. A uniform, stainless medium-grey colour indicates the effective activation of titanium alloys. In addition to this grey colour, Ti2Cu shows a characteristic longitudinal grain-flow.

Mechanism

The activation of titanium materials prior to plating is made possible by the selective dissolution/passivation activity of the activation solution.

With titanium alloys this selectivity means that:

The baser phase is dissolved

The surface topography generated by activation depends on the alloy and on its heat-treatment condition.

SALVAGE OF COMPONENTS

Adhesion

Plated parts withstand bend tests that deform the metal, machining and thermal shock. Quantitatively, the adhesion of deposits - determined by different adhesion tests (Figs. 1, 2) - ranges from 70-120 N/mm^2.

Application

Several engine parts out of dimension have been nickel plated or electroless nickel plated to salvage these components. Some examples are shown in Figs. 3-5. Thickness of nickel plating ranges from 0.1 to 0.6 mm (= 0.004-0.024 inch). Platings have been finished to dimensional shape by turning, milling or grinding.

Additionally to these machining operations, being good adhesion tests, plated test sheets have been prepared for determination of the adhesive strength.

TRIBOLOGY

The tribological characteristics of titanium in conjunction with electroplatings were investigated using a pin on disc apparatus and an oscillating wear tester (Figs. 6, 7).

Coefficient of friction

The coefficients of friction of electroplatings in conjunction with Ti6Al4V, determined in the pin on disc test, are shown in Table 3. If the coefficients of friction are compared with that of the Ti6Al4V-Ti6Al4V combination, it is revealed that the coefficient of friction of cobalt and cadmium in association with Ti6Al4V is lower than that of the Ti6Al4V combination, and the coefficient of friction of all the other combinations is higher than that of the combination Ti6Al4V-Ti6Al4V (μ = 0.45).

The tribological characteristics at room temperature can be changed at elevated temperature. Table 3 shows that at a temperature of 300 ^{o}C the coefficient of friction of the chromium - Ti6Al4V combination falls to 0.45 (30 ^{o}C μ = 0.65), while the coefficient of friction of the other combinations at 300 ^{o}C remain virtually unaffected.

Under the conditions of the oscillating test, the characteristics are somewhat different from those under sliding conditions. The major difference here being the rise in the coefficient of friction in relation to the number of cycles. This is particularly noticeable with the combination cobalt - Ti6Al4V, where the coefficient of friction increases from 0.3 to 0.85. The coefficient of friction is raised to 0.7-1.0 for all combinations.

Wear

Under sliding conditions, the wear characteristics of the Ti6Al4V pin against electroplatings differ according to the material of the countersurface. The wear is minimal against silver, copper and cobalt, moderate against electroless nickel and nickel, and maximal against chromium.

These wear characteristics of titanium at room temperature, in principle, do not change at a test temperature of 300 ^{o}C.

The wear of the Ti6Al4V under oscillating conditions is minimal against silver, slight against cobalt, moderate against copper, nickel and electroless nickel, high against chromium, and maximal against nickel composite coatings.

BEHAVIOUR AT ELEVATED TEMPERATURES

Adhesion

Adhesion of nickel platings can be improved by a heat treatment.

Heat treatment at 480 °C for 2 hours increases the adhesion of nickel on Ti6Al4V to 300 N/mm^2 and on Ti2Cu to 165 N/mm^2.

To improve adhesion of chromium on titanium temperatures of more than 750 °C are required.

Interdiffusion

The effects of heat treating the plating - titanium couples were examined after prolonged annealing at different temperatures. The results of interdiffusion were evaluated by light microscopy, and electron microprobe scans. In addition, phase determinations by these two techniques were confirmed by x-ray diffraction analysis. Depending on the plating and temperature, different effects can be observed.

Nickel or electroless nickel on titanium form Ti_2Ni and $TiNi_3$ by diffusion of nickel atoms into the base metal (Fig. 8). These compounds form two intermediate layers, which are inserted between the nickel coating and the titanium base metal in the order of nickel-$TiNi_3$-Ti_2Ni-titanium alloy. The formation of the third intermetallic compound, TiNi, theoretically possible according to the phase equilibrium diagram (2), has not been detected.

The diffusivity of nickel in titanium is remarkably high. In a 24 h treatment at 600 °C the diffusion distance, $\sqrt{4\,Dt}$ is 8 µm. This interdiffusion reaction starts already at temperatures of about 450 °C. As consequence of the high nickel diffusivity, Kirkendall voids are formed at the $TiNi_3$-Ni interface.

Cobalt or copper form a Ti_2Co or Ti_2Cu intermediate layer within an acceptable time at temperatures of 600 °C.

Chromium diffuses "normally" into titanium at temperatures of $\geq$750 °C.

Alloy	Alloying Constituents						Alloy Type
	Al	Cu	Sn	Mo	V	Zr	
Ti6Al4V	6	-	-	-	4	-	α , β
Ti2Cu	-	2	-	-	-	-	α
Ti6Al2Sn4Zr2Mo	6	-	2	2	-	4	α , β
IMI 685	6	-	-	0.8	-	5	α , β

Table 1 Titanium alloys

Step	Time (min)	Components	Temp. °C
Vapour degreasing	5	CCl_2 = CHCl (stab)	87
Blasting	-	Al_2O_3/270 mesh 4 bar	-
Pickling	15	HNO_3/HF	25
Activating	30	CrO_3/As_2O_3/HF	50
Plating	/um	Co/Cr/Cu/Ni/Ni-P	50

Table 2 Plating process

Coating	POD		SRV
	30°C	300°C	20°C
Ag	0.70	0.65	0.70 - 1.05
Cd	0.34	-	-
Co	0.30	0.27	0.2 - 0.85
Cr	0.65	0.43	0.6 - 0.7
Cu	0.8	0.63	0.6 - 0.7
Ni	0.85	0.75	0.65 - 0.75
Ni/P	0.46	0.43	0.55 - 0.8
Ni/P(400°C/1h)	0.59	0.57	0.6 - 0.65

Table 3 Coefficient of friction

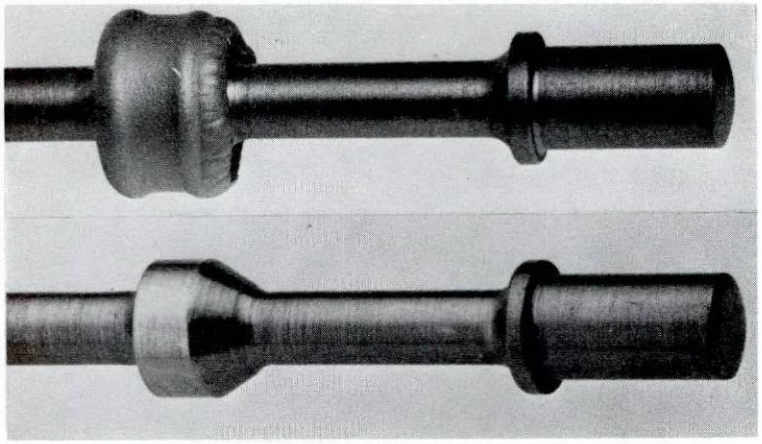

Fig. 3 0.1 mm Ni on Ti6Al4V, turned and ground

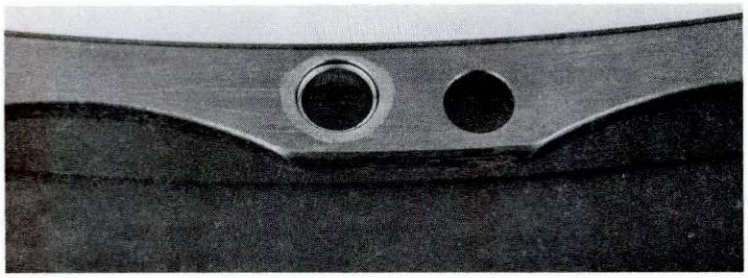

Fig. 4 0.15 mm Ni on Ti6Al4V, milled and bored

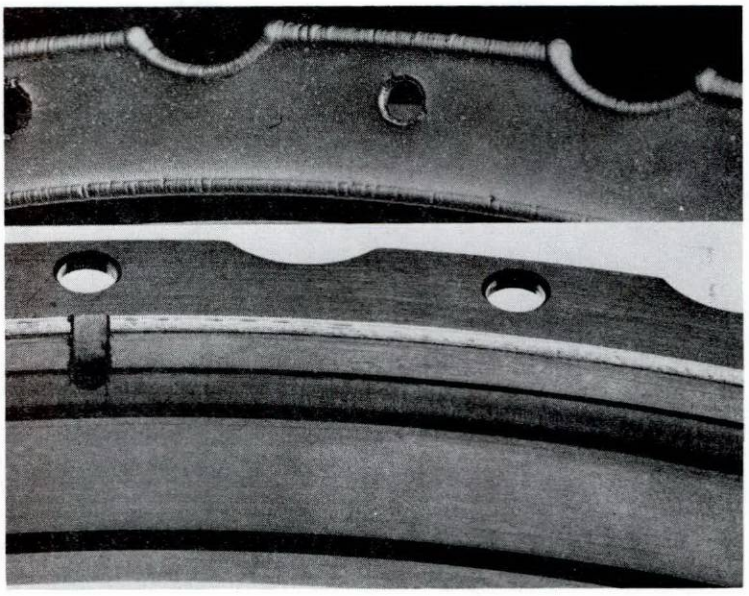

Fig. 5 Ni on IMI 685, turned

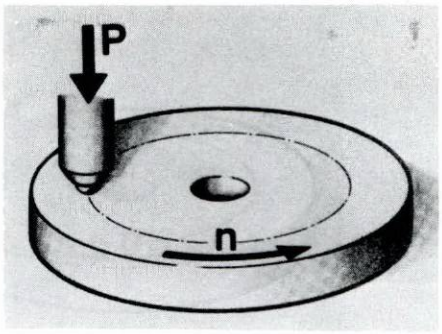

Fig. 6 Pin on disc

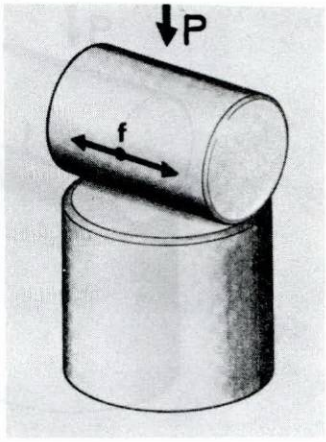

Fig. 7 Oscillating wear test

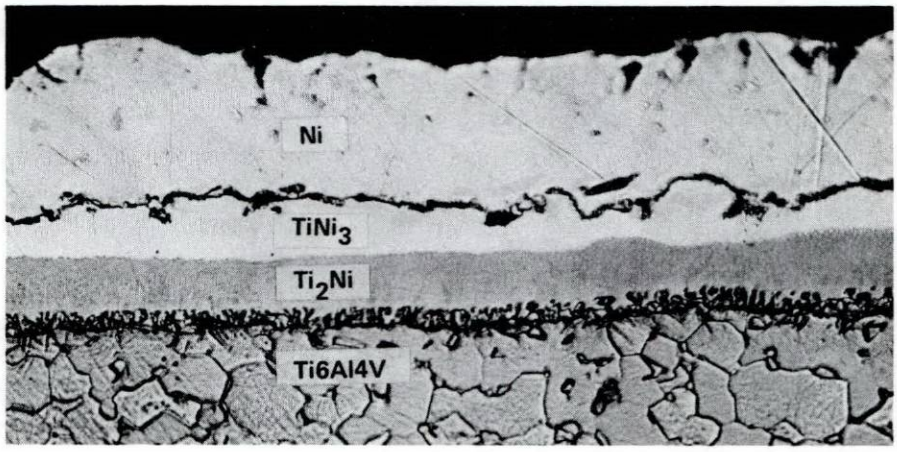

Fig. 8 Ni on Ti6Al4V, heat treatment 600 ^{o}C/100 h (x1000)


AMERICAN ELECTROPLATERS' SOCIETY